energies

MDPI

Article

Measurement Verification of a Developed Strategy of Inrush Current Reduction for a Non-Loaded Three-Phase Dy Transformer

Marian Łukaniszyn [1,*], Łukasz Majka [2,*,†], Bernard Baron [1], Barbara Kulesz [2], Krzysztof Tomczewski [1] and Krzysztof Wróbel [1]

[1] Department of Drive Automation and Robotics, Faculty of Electrical Engineering, Automatic Control and Informatics, Opole University of Technology, Prószkowska Street 76, 45-272 Opole, Poland
[2] Department of Electrical Engineering and Computer Science, Faculty of Electrical Engineering, Silesian University of Technology, Akademicka Street 10, 44-100 Gliwice, Poland; barbara.kulesz@polsl.pl
* Correspondence: m.lukaniszyn@po.edu.pl (M.Ł.); lukasz.majka@polsl.pl (Ł.M.)
† Participant in research fellowship at Department of Drive Automation and Robotics, Faculty of Electrical Engineering, Automatic Control and Informatics, Opole University of Technology.

Abstract: This article presents the measurement verification of a novel strategy for inrush current reduction in an unloaded three-phase Dy transformer. The strategy combines appropriate pre-magnetization of transformer cores with an original control switching system using initial phase values of the supply voltage as control variables. Measurements were recorded for primary voltages and currents as well as secondary voltages during transient states at start-up under no-load conditions. Various inrush scenarios were examined across the full angular spectrum of initial phase angles, both polarities, and in regard to different pre-magnetization current values. A detailed analysis of the inrush currents was performed using proprietary automated software based on the recorded data. A comparative study with a nonlinear mathematical model of the transformer was also conducted. Additionally, key technical aspects of the designed system for implementing the proposed pre-magnetization strategy with controlled voltage energization are discussed.

Keywords: three-phase Dy transformer; inrush current phenomenon; strategy of pre-magnetization of the transformer cores; controlled voltage energization; electromagnetic transients; measurement verification

check for updates

Citation: Łukaniszyn, M.; Majka, Ł.; Baron, B.; Kulesz, B.; Tomczewski, K.; Wróbel, K. Measurement Verification of a Developed Strategy of Inrush Current Reduction for a Non-Loaded Three-Phase Dy Transformer. *Energies* **2024**, *17*, 5368. https://doi.org/10.3390/en17215368

Academic Editors: Dan-Cristian Popa and Ioana-Cornelia Gros

Received: 15 September 2024
Revised: 22 October 2024
Accepted: 23 October 2024
Published: 28 October 2024

Copyright: © 2024 by the authors. Licensee MDPI, Basel, Switzerland. This article is an open access article distributed under the terms and conditions of the Creative Commons Attribution (CC BY) license (https://creativecommons.org/licenses/by/4.0/).

1. Introduction

The issue regarding transformer inrush currents (identification and mitigation techniques) has been known and investigated for a long time. Studies are still under way [1–3]. When a transformer is energized, an inrush current is generated and its amplitude and harmonic content are high. The presence of an inrush current can mislead the transformer protection so that the circuit may be broken without necessity. This will prolong the transformer's energization process and increase the number of times the transformer windings may be subjected to undesirable mechanical stress [4,5]. This current adversely affects the power system, decreasing its reliability. It also damages the transformer, causing a reduction in its lifetime and leading to the maloperation of the protective relay.

Therefore, several studies have been carried out on the inrush current of a transformer. The techniques proposed in [6–9] can improve the ability to distinguish between inrush and fault currents. References [3,10–15] studied the inrush current-mitigating techniques. Studies on the controlled energization of transformers can be found in [16–20].

This article presents a comprehensive approach to modeling a distribution transformer with a primary focus on developing an effective strategy to reduce inrush currents during transformer energization. The study emphasizes practical implementation and stands out by offering a complete solution that encompasses the concept, methodology, tools, and mathematical models, all based on minimal input data. The data required for this model

can easily be obtained from standard measurements of the transformer itself, making the approach highly accessible and practical for professional engineers.

The authors' model has been validated on a real object. The validation distinguishes the current study from previous works. This novel approach is particularly useful for analyzing the transient states of the transformer, such as calculating current pulses during the energization of an unloaded transformer. The necessity for such research arises from the growing complexity of distribution systems caused by the increasing integration of renewable energy resources and energy storage devices [21,22].

The detailed presentation of the mathematical model highlights its utility in addressing challenges in modern power distribution, providing engineers with a reliable tool to enhance transformer performance and mitigate inrush current issues effectively.

This model does not account for magnetic hysteresis, as it does not track the 'history' of core magnetization, meaning it does not consider the points at which the directions of current and magnetic flux reverse. However, the magnetization history of the core can be specified solely for the moment of transformer energization in the form of residual magnetism. In the model under consideration, the presence of residual magnetism is accurately accounted for in all columns of the transformer core. Therefore, if the residual magnetism is known, it is possible to set the initial conditions in the form of the state variables $\Psi_k(t_0)$, which represent the flux linkages of the primary (energized) windings $\Psi_k(t_0) = B_k s_{\mathrm{Fe}} N_1$, where B_k is a residual flux density in the transformer core's different columns (for all symbols used in this paper—see Abbreviations). By performing integration under these initial conditions, the first entry into the core saturation region is calculated. Since this region is where the largest current pulses occur, the obtained solution is highly accurate.

The variable t_0 in the equations represents a parameter that is varied according to the instantaneous values of the supply voltages $u_{12} = |E_m| \sin(\omega t_0 + \frac{2\pi}{3})$, $u_{23} = |E_m| \sin(\omega t_0 + 0)$ and $u_{31} = |E_m| \sin(\omega t_0 + \frac{4\pi}{3})$. This approach allows for calculations that account for the impact of the moment when the voltage is applied to the unloaded transformer, measured relative to the moment when the reference voltage $u_{23}(t)$ crosses zero.

This study primarily focuses on the comparative analysis of measurement and simulation waveforms during the initial phase of the transient state caused by energizing an unloaded transformer. The analysis relies on an improved model that has been refined through experimental research and previously developed practical modifications (see [23]). The inrush scenarios were recorded for varying initial phase angles of the supply voltage, covering the entire 0–360-degree spectrum in 10-degree increments, for both polarities of the pre-magnetization current (positive and negative) and with currents ranging from approximately 0.7 of the no-load current up to 1.3 of its rated value.

The comparisons include voltage and current waveforms on both the primary and secondary sides of the transformer, focusing on the accuracy of reproduced current pulse magnitudes observed in 72 instances (2 magnetization polarities $\times$ 36 phase angle changes) in the inrush scenarios, including their peak values. The study also examines deformations in induced voltages on the secondary side and their influence on the primary side. Due to the complexity and number of attributes involved in assessing the conformity between recorded and calculated results, graphical analysis serves as the most effective and comprehensible approach to illustrating these results.

This article concludes and wraps up a triplet series dedicated to the dynamics of inrush currents in three-phase Dy transformers. The series progresses from the initial strategy and simulations presented in [24] through the practical experiments and refinements in [23] before reaching the current phase of empirical measurement verification. The methods described have been fully implemented and validated across the full range of operational conditions, solidifying the practical application of the research findings.

As the final installment, this article encapsulates the entire process from theoretical strategy development to practical and measurement-based verification, emphasizing the robust implementation of the methods investigated throughout the publication cycle.

2. Model of Unloaded Three-Phase Dy Transformer

To compare and verify the measurement results of the mathematical modeling, it is first necessary to present the structure and properties (assumptions) of the considered mathematical model. This model is the original work of the authors and has been developed entirely from scratch. During the conducted simulations and experimental studies, the model has been continuously updated and its functionality has been validated [23,24].

2.1. Model Principles

In its current form, it is fully suitable for achieving the originally intended two objectives: 1* reliable simulation of inrush currents occurring during the initial period of the transient state in a 3-phase Dy transformer being energized under no-load conditions; 2* practical implementation of any simulation scenario (strategy) for energizing the transformer with full control over the generated inrush current pulses (primary objective is to minimize these currents). The equivalent circuit of this model is shown in Figure 1.

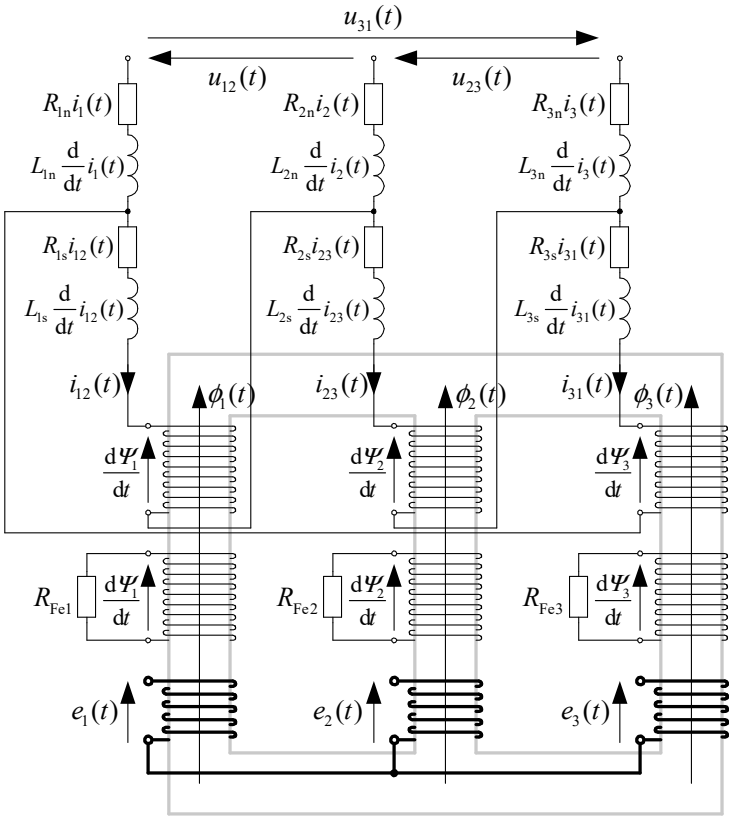


Figure 1. Circuit model of the considered three-phase Dy transformer in unloaded state.

2.2. Nonlinear Characteristic of the Ferromagnetic Core

The model takes into account the nonlinear magnetization curve $\Psi(I_0)$ in the form of a polynomial approximation using odd powers (1) of the original $B(H)$ curve provided by the transformer sheet manufacturer [19].

$$H(B) = \sum_{k=1}^{11} a_k B^{2k-1} \tag{1}$$

The approximation was performed using an 11th-degree polynomial. The choice of method (polynomial approximation) is natural/obvious in the context of the classical method for solving systems of overdetermined equations. The odd degree arises from the requirement that the function must be symmetric with respect to the center of the coordinate system. The high order significantly enhances the reproduction of points

beyond the saturation knee, a crucial region for analyzing extreme saturation states of the core in inrush scenarios. Accurate mathematical representation of this saturation region is essential, as current pulses occur when the core initially enters saturation.

The most significant model implementations included solutions that allow for the consideration of residual magnetism in individual core columns and control over the precise timing of voltage switch-on, also in relation to the voltages of all three phases [24].

The authors' model is described by nonlinear differential equations which are classified as stiff equations. The nature of such equations is specific, and the numerical solution process is highly demanding (high computational cost). It requires the use of an original approach (including custom numerical libraries and original implementations of the Runge–Kutta and Radau methods) and specific solution techniques (e.g., solutions incorporating approximations determined within the limit cycle). Due to the use of a specialized, proprietary solver dedicated to the issue of stiff equations, the developed mathematical model of the transformer can also be used to determine the steady state [25,26].

3. Residual Magnetism

Since it is difficult to measure the value of residual magnetism [27–30] necessary for formulating initial conditions in simulations, we decided that the exact value could be entered manually (artificial setting) instead of putting in the measured value. This approach ensures the preliminary magnetization of the core to a known or estimable value. The preliminary magnetization of the columns of the tested transformer was carried out in the setup shown in Figure 2.

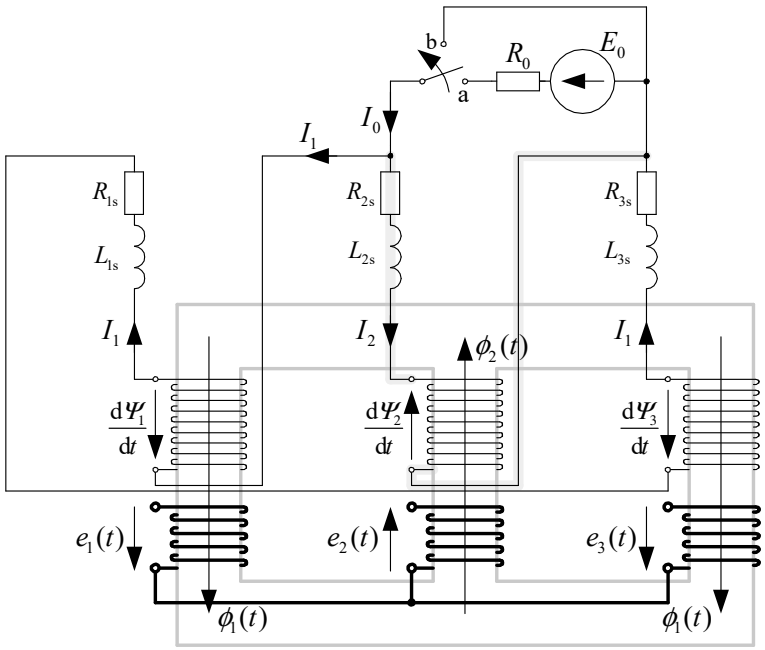


Figure 2. Diagram of the system for pre-magnetization of transformer core limbs (it is also used for the windings' DC current decay test).

The starting point for the practical implementation of the intended task is based on the guidelines provided in [24]. A DC voltage source with a adjustable current (a rheostat is used) is connected to the terminals of the primary winding in the central column of the transformer (in place of the reference voltage $u_{23}(t)$). The configuration of the primary winding connections (delta connection) remains intact.

The value of the current I_0 is set slightly above the no-load current value. The current I_0 supplied by the source flows through the windings arranged in a series-parallel circuit. Since the winding resistances are identical, the current distribution is symmetrical.

$$I_2 = \frac{2}{3}I_0\,,\; I_1 = I_3 = \frac{1}{3}I_0\,,\; I_0 = I_1 + I_2 \tag{2}$$

Such a distribution of direct currents ensures magnetization of the individual transformer columns in the following proportions:

$$B_1 = -\frac{1}{2}B_0, B_2 = B_0, B_3 = -\frac{1}{2}B_0 \tag{3}$$

The proportions may be changed if the direction of current I_0 in the setup shown in Figure 2 is reversed.

This arrangement is well illustrated by the magnetic circuit diagram of the transformer model for the steady state (Figure 3), which confirms the above finding.

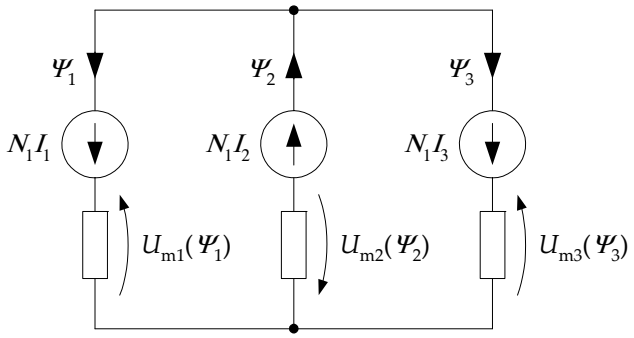


Figure 3. Equivalent diagram of the magnetic circuit of a three-phase transformer after applying pre-magnetization (duplicated open access resource [23]).

If the value of DC current I_0 exceeds the amplitude of the transformer's no-load current (see diagram in Figure 2), then magnetization and eventual saturation of the magnetic core in the transformer's columns will follow. In the experiment aimed at determining the value/level of magnetization, the induced voltages on the secondary side of the transformer $e_k(t)$ (Figure 2) are recorded during the decay of current in the primary windings [31]. This decay is caused by short-circuiting the powered windings while simultaneously disconnecting the source (as illustrated in Figure 2 by switching the breaker from position 'a' to position 'b'). In this process, the magnetic fluxes $\Phi_k(t)$ in the individual transformer columns (Figure 2) also change. According to Faraday's Law, these flux changes induce voltages in the secondary windings of the transformer.

By adapting the magnetic flux density in the windings of the individual transformer columns, the following can be expressed

$$\Phi_k(t) = B_k(t)s_{\mathrm{Fe}} \tag{4}$$

Changes in these fluxes, in accordance with Faraday's Law, cause voltages to be induced on the secondary side of the transformer with N_2 number of turns [32,33]

$$\frac{\mathrm{d}}{\mathrm{d}t}\Phi_k(t) = \frac{1}{N_2}e_{k(\mathrm{s})}(t) \tag{5}$$

Finally

$$\frac{\mathrm{d}}{\mathrm{d}t}B_k(t) = \frac{1}{N_2 s_{\mathrm{Fe}}}e_{k(\mathrm{s})}(t) \tag{6}$$

By performing the operation of integrating the equations while taking into account the initial conditions in the form of $B_k(0)$, one obtains

$$B_k(t) = B_k(0) + \frac{1}{N_2 s_{\mathrm{Fe}}} \int_0^t e_{k(\mathrm{s})}(\tau)\mathrm{d}\tau \tag{7}$$

where

$$B_k(0) = \frac{\Psi_k}{N_2 s_{\mathrm{Fe}}} \tag{8}$$

The results obtained through this practical (measurement–calculation) approach can be derived from the numerical solution of the system of nonlinear equations based on Kirchhoff's first and second laws for the magnetic circuit shown in Figure 3

$$\begin{bmatrix} f_1(\boldsymbol{X}) \\ f_2(\boldsymbol{X}) \\ f_3(\boldsymbol{X}) \end{bmatrix} = \begin{bmatrix} I_0 N_1 - U_{\mathrm{m},2}(\Psi_2) - U_{\mathrm{m},1}(\Psi_1) \\ I_0 N_1 - U_{\mathrm{m},2}(\Psi_2) - U_{\mathrm{m},3}(\Psi_3) \\ \Psi_2 - \Psi_1 - \Psi_3 \end{bmatrix} = 0 \tag{9}$$

where $U_{\mathrm{m},k}$ represents the magnetic voltage drop.

When this system of nonlinear equations is solved, then flux linkages $\Psi_k(t)$ are determined; subsequently, corresponding magnetic flux density values $B_k(t)$ are obtained.

4. Initial Magnetization

Regarding the measurements, the influence of the pre-magnetization current value on the residual magnetism was investigated. This was accomplished using a proprietary device designed for controlled transformer energization (with a specific initial phase of the reference voltage—this issue will be discussed later). Different values of the current were set, reaching values exceeding the transformer's no-load current. For each specified current value, the decaying current in the primary windings and the electromotive forces induced at the secondary winding terminals were recorded. If it is necessary to filter the measured waveforms, the optimal SASS method [34] can be used for these transient signals with discontinuities. When the instantaneous values of the induced voltages on the transformer's secondary side $e_k(\tau)$ are given, the result of the integration, according to Equation (7), yields the corresponding magnetic flux density values $B_k(t)$ for the transformer's columns. In the limiting case, the magnetic flux density values correspond to the point on the magnetic hysteresis curve (flux density value) of residual magnetism for the transformer's central column [19], $B_k = \lim_{t\to\infty} B_k(t)$ (Figure 4).

The measurements conducted for several values of $B_2(0)$ associated with the initial magnetization of the transformer core, and corresponding to current I_0 values (see Table 1), proved that the initial magnetization value is independent of the magnetizing current (remaining practically unchanged for values exceeding the no-load current). The limits $B_k = \lim_{t\to\infty} B_k(t)$ are approximately the same; for the discussed transformer, they are equal to $B_2 = 1\,\mathrm{T}$. This represents the magnetic hysteresis value for the transformer's central column. For the outer columns, these values are approximately $B_1 = B_3 = -\frac{1}{2}B_2$.

Table 1. Initial flux density values obtained during calculation based on measurement waveforms (DC decay test) recorded for carefully chosen values of the magnetization current (greater than the no-load current value).

I_0, mA	160	287	395	481
$B_2(0)$, T	1.809	1.835	1.878	1.893

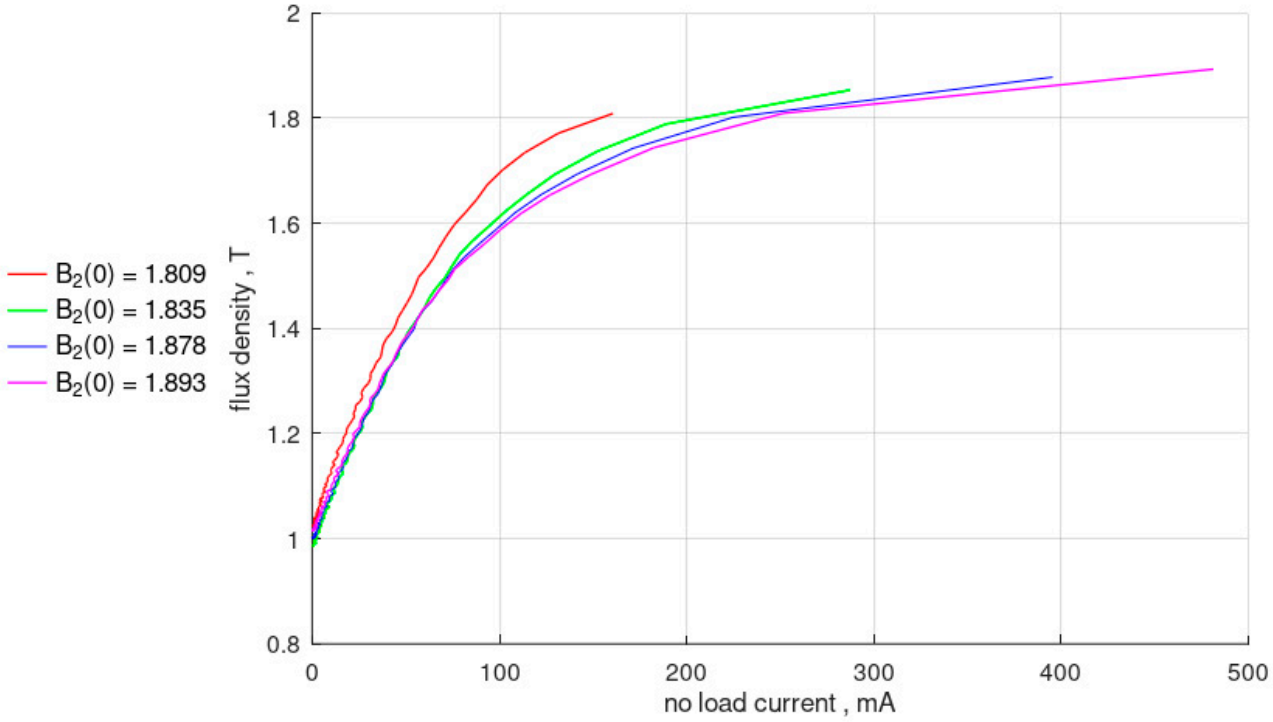


Figure 4. Set of flux density curves against current obtained for the carefully chosen values of the magnetization current.

Using the proprietary device for controlled energization (where the transformer is energized at a specified instant of the reference voltage $u_{23}(t)$), the impact of the pre-magnetization current on the maximum generated inrush current of the transformer was examined (Table 2).

Table 2. Maximum values of transformer's inrush current depending on the pre-magnetization current.

I_0, mA	0.1	0.3	0.6	1.2	1.8	2.1	2.4
I_{max}, A	30.4498	30.0584	30.0836	30.1146	29.8151	30.4899	29.962

Measurements indicated that the peak value of this current is practically independent of the magnetizing current if it exceeds 0.1 A (no-load current value). This means that, if the transformer's core is magnetized with a current exceeding this value, the hysteresis will be stabilized when the current decays to zero (see Figure 2, switch set to 'b' position).

The practical experiment was validated through simulation studies. Calculations of the maximum current values were conducted under the same switching conditions (identical time instant in the reference voltage) while the initial magnetization value was changed. The simulation studies have shown that the maximum current pulse of 30 A is obtained when the initial values for calculations are input in accordance with (2), i.e., for $B_0 = 1\,\mathrm{T}$. This indirect approach allowed for the approximate identification of the residual magnetism values with proportions specified in/given by (3). Therefore, it is beyond doubt that the decrease in current in the windings to zero accompanying the changes in magnetic fluxes induced by the DC magnetization of the core columns ultimately leads to the stabilization of flux density values corresponding to residual magnetism.

As demonstrated in studies [24], the best approach for initial magnetization is to maintain a certain symmetry; this is evident in the circuit shown in Figure 3. In this system, the flow of direct current ensures magnetization in the individual columns of the transformer in guaranteed proportions (3).

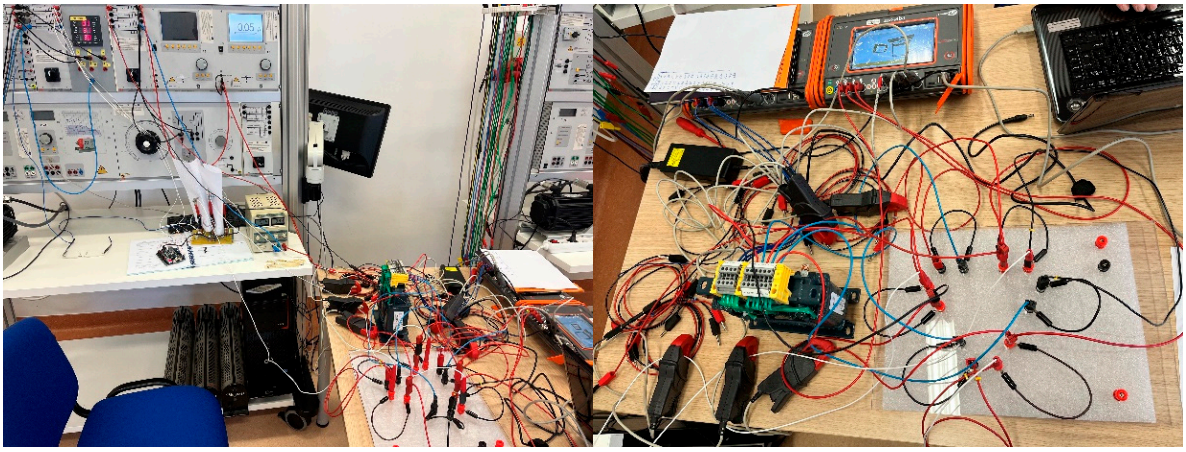
If the direction of current I_0 in the system shown in Figure 2 is reversed, the magnetization symmetry will be preserved but with an opposite polarity

$$B_2 = -B_0\,,\; B_1 = B_3 = \frac{1}{2}B_0 \tag{10}$$

These values form the basis for calculating transformer current pulses in the no-load state after the device is energized. Such values of residual magnetism B_k will be considered in all numerical experiments (with $B_k(0)$ as initial conditions for integration). Results of numerical experiments will be compared with measurement results. The developed symmetry of initial magnetization ((3) and (9)) ensures that the resulting pulses upon the transformer's connection to the grid maintain the same timing regardless of the sequence of the supply voltage phases.

5. Laboratory Setup

The experiments were conducted using a measurement setup designed specifically for this purpose. The setup includes the following components: a tested three-phase Dy11 transformer, a power circuit switch, a regulated DC power supply, a thyristor controller synchronized with the zero-crossing signal of the phase voltage, and two six-channel event recorders (with a sampling frequency of more than 10 kHz per channel). Photos of the setup are presented in Figure 5 while the schematic diagram of the implemented DC and AC power switching is shown in Figure 6. The power circuit switch consists of a three-phase AC_{ON}, which connects the AC voltage source to the system, and a DC_{ON} switch, which applies the magnetizing current to the winding.



(**a**) (**b**)

Figure 5. General view of the laboratory measurement setup (**a**) and the connection layout of the investigated transformer (**b**).

The magnetization of the columns of the tested transformer is carried out according to the diagram (Figure 6), which fully corresponds to the diagram (Figure 2).

The tested transformer was powered from the mains through triacs, which were triggered at a specified phase angle of the supply voltage applied to the winding of the central column. The power circuit switches in the system allow for the connection of the setup either to the mains or to a DC power supply used for magnetizing the core before each application of the mains voltage. A special controller enables the setting of the phase angle of the supply voltage for the central column winding of the transformer. The thyristors are triggered at this particular angle/time instant in a reference sine wave. The block diagram of the controller is shown in Figure 7.

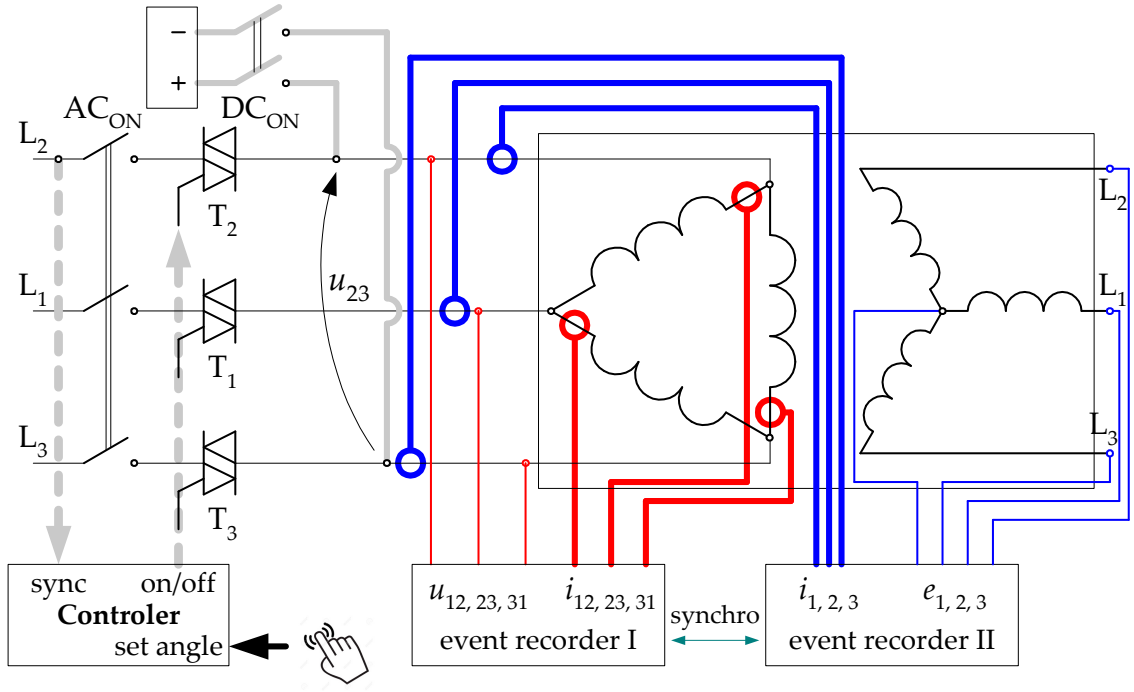


Figure 6. The schematic diagram of the implemented DC/AC power switching—implementation of the initial magnetization connections of the tested transformer.

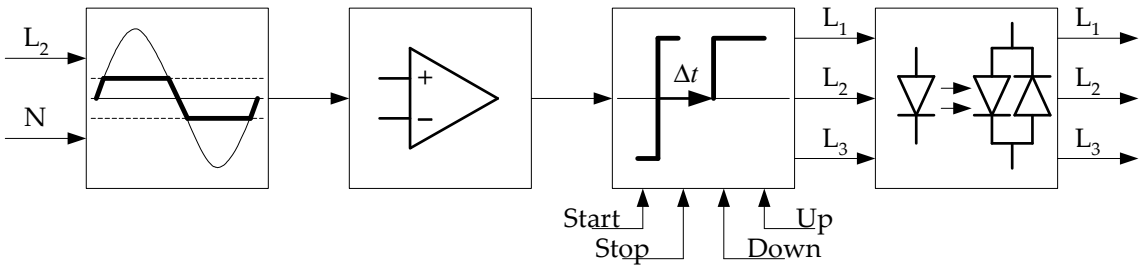


Figure 7. Block diagram of the original controller.

The user interface consists of four buttons and a display. They are used for setting the phase angle value as well as switching thyristors $_{ON}/_{OFF}$. To determine the phase angle for thyristor triggering, a voltage limiter and comparator are used at the input of the controller. The signal from the comparator output is fed to a Spartan 3 programmable logic device, which triggers the triacs with a delay proportional to the phase angle value. The signal from the FPGA outputs is then sent to the inputs of the optotriacs, which provide a galvanic isolation between the controller part and power part of the circuit.

Before each application of the supply voltage, the transformer core was magnetized with a direct current of a specified value and flow direction. After disconnecting the DC power supply, the mains voltage was applied. The delay in triac activation was determined by the controller based on the previously set phase angle value.

Measurements were carried out using two six-channel recorders. The recorded data included the waveforms of voltages and currents in the primary windings of the transformer and the supply lines, as well as the voltages in the secondary windings.

The collected measurement data contain/include recordings made for both directions of the magnetizing current flow (polarization) across the full phase angle range (angle incremented by 10 deg). Additionally, separate recordings were made for selected phase angles and various magnetizing current values ranging from 0.1 to 2 A with increments of 0.1 A.

6. Calibration Measurement—Updating Magnetic Circuit Diagram

For the purpose of calibrating the system, the individual columns of the transformer were pre-magnetized in accordance with (3). Then, a three-phase supply was connected with a correct phase sequence. The connection was made at a precisely defined moment, corresponding to the zero-crossing of the reference voltage $u_{23}(t)$.

The discretely recorded waveforms of the instantaneous voltages $u_{k,l}(t)$ and currents $i_{k,l}(t)$ on the primary side of the transformer (currents in delta winding) are presented in Figure 8, along with intentionally recalculated secondary side voltages $e_k(t)$ (for comparison purposes). To achieve this, the previously established principle was utilized. It states that, based on the voltage $e_k(t)$ waveforms induced in the N_2 windings of the unloaded secondary side, one can determine the waveforms of the voltages induced in the N_1 windings of the primary side. In modeling, these correspond to the time derivates of flux linkages $\frac{\mathrm{d}}{\mathrm{d}t}\Psi_k(t)$ (see Figure 1), which are given by

$$\frac{\mathrm{d}}{\mathrm{d}t}\Psi_k(t) = r_{\mathrm{N}} e_{k(\mathrm{s})}(t) \tag{11}$$

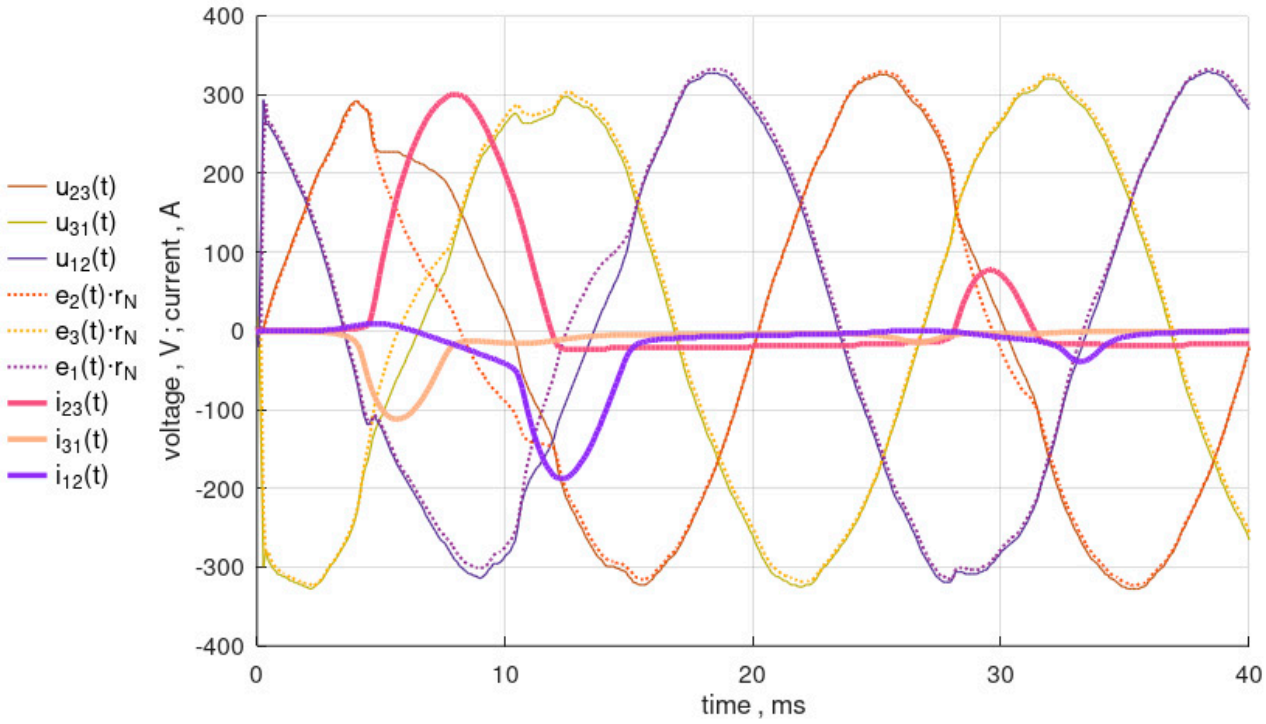


Figure 8. Measured and recorded waveforms of all three delta currents $i_{k,l}(t)$ of the transformer's primary windings—inrush currents of the unloaded transformer in the first period of the transient state and all primary voltages $u_{k,l}(t)$ as well as all secondary voltages $e_k(t)$ intentionally rescaled by transformer winding ratio $\mathrm{r_N}$; energizing occurred with residual magnetism in variant $B_1 = -\frac{1}{2}B_0$, $B_2 = B_0$, $B_3 = -\frac{1}{2}B_0$; the reference supply voltage $u_{23}(t)$ applied to the transformer center column winding of the unloaded Dy transformer exactly at the time instant when voltage $u_{23}(t)$ crosses zero.

As can be observed, the waveforms $u_{k,l}(t)$ differ significantly from the waveforms $e_k(t) \cdot \mathrm{r_N}$ in the time intervals where current pulses $i_{k,l}(t)$ occur.

This is due to the fact that (based on Figure 1)

$$\begin{aligned} u_{12}(t) - L_{1\mathrm{s}}\tfrac{\mathrm{d}}{\mathrm{d}t}i_{12}(t) - R_{1\mathrm{s}}i_{12}(t) - r_{\mathrm{N}}e_{1(\mathrm{s})}(t) &= 0 \\ u_{23}(t) - L_{2\mathrm{s}}\tfrac{\mathrm{d}}{\mathrm{d}t}i_{23}(t) - R_{2\mathrm{s}}i_{23}(t) - r_{\mathrm{N}}e_{2(\mathrm{s})}(t) &= 0 \\ u_{31}(t) - L_{3\mathrm{s}}\tfrac{\mathrm{d}}{\mathrm{d}t}i_{31}(t) - R_{3\mathrm{s}}i_{31}(t) - r_{\mathrm{N}}e_{3(\mathrm{s})}(t) &= 0 \end{aligned} \tag{12}$$

The conducted experimental studies demonstrated that the sum

$$r_{\mathrm{N}}\left(e_{1(\mathrm{s})}(t)+e_{2(\mathrm{s})}(t)+e_{3(\mathrm{s})}(t)\right)=\frac{\mathrm{d}}{\mathrm{d}t}\Psi_1(t)+\frac{\mathrm{d}}{\mathrm{d}t}\Psi_2(t)+\frac{\mathrm{d}}{\mathrm{d}t}\Psi_3(t)\neq 0 \tag{13}$$

is different from zero (Figure 9), particularly in the initial interval where current pulses occur upon the transformer's energization [35].

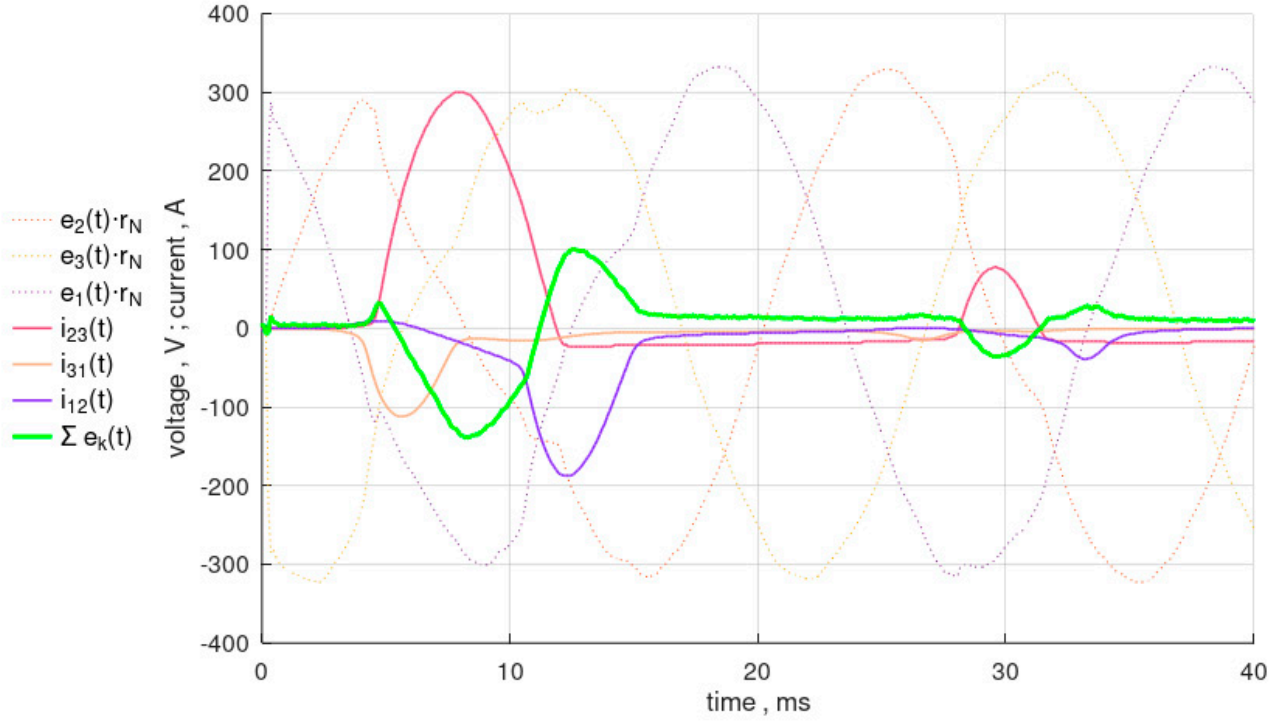


Figure 9. The dynamic waveform of the unbalanced sum of secondary winding voltages multiplied by the winding ratio calculated from the measured and recorded waveforms during transformer energizing shown in Figure 8; the correspondence of the unbalanced sum to the inrush current pulses is seen.

This finding indicates that, when modeling the transformer circuit during such transient states, Kirchhoff's first law cannot be applied to the magnetic circuit in the form $\Psi_1(t)+\Psi_2(t)+\Psi_3(t)=0$. To develop a proper solution, taking into account this phenomenon, an introduction of a special (air) magnetic shunt in the transformer's core columns within the circuit model might be considered [23]. The magnetic resistance (reluctance) of this shunt could be determined based on Figure 10.

To determine the value of the magnetic shunt's reluctance $R_{\mathrm{m}\delta}$, a criterion linking measurement with simulation was established. The value of the shunt's reluctance is selected based on the conformity between the measured value

$$\max_{t\in[0,\mathrm{T}]}\left\{r_{\mathrm{N}}\left(e_{1(\mathrm{s})}(t)+e_{2(\mathrm{s})}(t)+e_{3(\mathrm{s})}(t)\right)\right\} \tag{14}$$

and the value

$$\frac{\mathrm{d}}{\mathrm{d}t}\Psi_1(t)+\frac{\mathrm{d}}{\mathrm{d}t}\Psi_2(t)+\frac{\mathrm{d}}{\mathrm{d}t}\Psi_3(t)=\frac{\mathrm{d}}{\mathrm{d}t}(\Psi_1(t)+\Psi_2(t)+\Psi_3(t)) \tag{15}$$

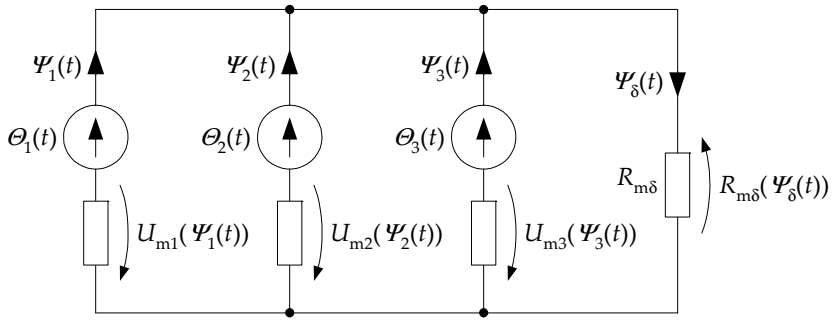


Figure 10. The equivalent magnetic circuit diagram of the unloaded three-phase transformer during magnetization (after applying pre-magnetization) updated by adding a shunt to account for unbalanced residuals of the fluxes leaking from the core and closing beyond it, e.g., through the air (duplicated open access resource [23]).

obtained from computer simulations, minimizing the sum of the squared differences.

It is important to emphasize that, in the experiment, it is absolutely necessary to introduce the initial magnetization of the transformer core columns to enable a valid comparison between the simulation results and the measurements on the actual object (ensuring an identical reference setup).

The best measurement deviation results (Figure 11), in accordance with Equations (14) and (15), were used to determine thr magnetic reluctance of the air magnetic shunt $R_{m\delta}$ (see Figure 10). It was calculated under the same test conditions as those shown in Figure 8, i.e., at the moment when the voltage $u_{23}(t)$ crosses zero. It was calculated as $R_{m\delta} = 4\,420\,970\ \frac{A}{Wb}$.

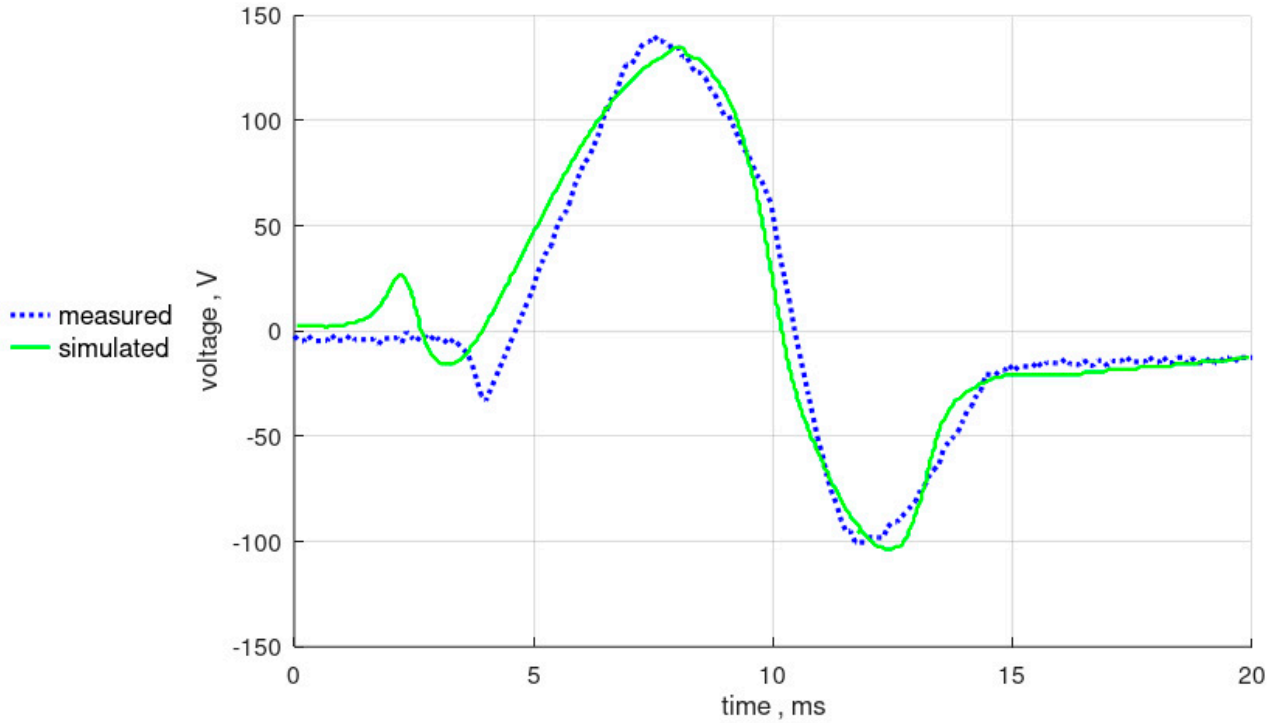


Figure 11. Comparison of the results of the calculated sum of the electromotive forces of self-induction in the primary winding (numerically determined $\frac{d}{dt}\Psi_1(t) + \frac{d}{dt}\Psi_2(t) + \frac{d}{dt}\Psi_3(t)$) with the sum of the electromotive forces of self-induction in the secondary windings of the transformer (derived from the tests and multiplied by the transformer ratio $r_N\left(e_{1(s)}(t) + e_{2(s)}(t) + e_{3(s)}(t)\right)$).

The waveform obtained from the measurement serves as a reference point in the process of estimating the value of the reluctance $R_{m\delta}$ present in the mathematical model. The estimation algorithm adjusts the value of this element by minimizing the deviations between the simulated and measured waveforms. In practical implementation, a comparison between measured and simulated waveforms can be made using a variety of criteria (for instance, as in [36], when sums of squares are used or through an integral error [37]).

7. Nonlinear Differential Equations for Transformer Transient State Computations

For the updated transformer model (with magnetic resistance $R_{m\delta}$ in the form of an air shunt), based on Kirchhoff's second law for the magnetic circuit shown in Figure 10, the following equations are obtained:

$$\begin{array}{l} \Theta_1(t) - U_{m,1}(\Psi_1(t)) - R_{m\delta}(\Psi_1(t) + \Psi_2(t) + \Psi_3(t)) = 0 \\ \Theta_2(t) - U_{m,2}(\Psi_2(t)) - R_{m\delta}(\Psi_1(t) + \Psi_2(t) + \Psi_3(t)) = 0 \\ \Theta_3(t) - U_{m,3}(\Psi_3(t)) - R_{m\delta}(\Psi_1(t) + \Psi_2(t) + \Psi_3(t)) = 0 \end{array} \tag{16}$$

where magnetic voltage drops are defined by

$$U_{m,k}(\Psi_k(t)) = h_{Fe,k} H \frac{\Psi_k(t)}{N_1 s_{Fe}} \tag{17}$$

The magnetomotive forces of the individual windings on the primary side of the transformer can be expressed as

$$\begin{array}{l} \Theta_1(t) = \left(i_{12(p)}(t) - i_{Fe,1}(t)\right) N_1 \\ \Theta_2(t) = \left(i_{23(p)}(t) - i_{Fe,2}(t)\right) N_1 \\ \Theta_3(t) = \left(i_{31(p)}(t) - i_{Fe,3}(t)\right) N_1 \end{array} \tag{18}$$

In the model shown in Figure 1, it is assumed that the resistances $R_{Fe,k}$ represent the total power losses in the transformer's core. It is also assumed that the flux derivative $\frac{d}{dt}\Psi_k(t)$ is the electromotive force at the terminals of the coil with N_1 turns and zero resistance. This coil is wound around thr k-th column of the transformer and is shorted by $R_{Fe,k}$ resistance

$$\frac{d}{dt}\Psi_k(t) = R_{Fe,k} i_{Fe,k}(t) \tag{19}$$

Model parameters $R_{Fe,k}$ may be determined by measuring the active power of the transformer at no-load and under steady-state conditions. It is worth mentioning that this mathematical model of the transformer may be used to determine the steady-state of the transformer as the limit cycle of the solution of the differential equation system describing the operation of the transformer [25,26,38].

The currents $i_{Fe,k}(t)$, simulating iron losses (see Equation (19)), are substituted into Equation (18), and then the resulting magnetomotive forces (MMFs) $\Theta_k(t)$ are substituted into Equation (16). After transformation, the following expression is obtained

$$\begin{array}{l} \frac{d}{dt}\Psi_1(t) = R_{Fe,1} i_{12(p)}(t) - \frac{R_{Fe,1}}{N_1}(U_{m,1}\Psi_1(t) + R_{m\delta}(\Psi_1(t) + \Psi_2(t) + \Psi_3(t))) \\ \frac{d}{dt}\Psi_2(t) = R_{Fe,2} i_{23(p)}(t) - \frac{R_{Fe,2}}{N_1}(U_{m,2}\Psi_2(t) + R_{m\delta}(\Psi_1(t) + \Psi_2(t) + \Psi_3(t))) \\ \frac{d}{dt}\Psi_3(t) = R_{Fe,3} i_{31(p)}(t) - \frac{R_{Fe,3}}{N_1}(U_{m,3}\Psi_3(t) + R_{m\delta}(\Psi_1(t) + \Psi_2(t) + \Psi_3(t))) \end{array} \tag{20}$$

Equation (20) demonstrates that circuit modeling of the transformer for the analysis of such transient states as those accompanying the energization of an unloaded transformer requires taking into account all column flux linkages $\Psi_k(t)$.

At the next stage of modeling, in accordance with Kirchhoff's second law, three equations corresponding to the independent loops on the primary side of the transformer (Figure 1) are considered, and they take the following form:

$$\begin{gathered}
u_{12}(t) - R_{1n}i_1(t) - L_{1n}\frac{d}{dt}i_1(t) - R_{1s}i_{12}(t) - L_{1s}\frac{d}{dt}i_{12}(t) - \\
-\frac{d}{dt}\Psi_1(t) + R_{2n}i_2(t) + L_{2n}\frac{d}{dt}i_2(t) = 0 \\
u_{23}(t) - R_{2n}i_2(t) - L_{2n}\frac{d}{dt}i_2(t) - R_{2s}i_{23}(t) - L_{2s}\frac{d}{dt}i_{23}(t) - \\
-\frac{d}{dt}\Psi_2(t) + R_{3n}i_3(t) + L_{3n}\frac{d}{dt}i_3(t) = 0 \\
R_{1s}i_{12}(t) + L_{1s}\frac{d}{dt}i_{12}(t) + \frac{d}{dt}\Psi_1(t) + \\
+R_{2s}i_{23}(t) + L_{2s}\frac{d}{dt}i_{23}(t) + \frac{d}{dt}\Psi_2(t) + R_{3s}i_{31}(t) + L_{3s}\frac{d}{dt}i_{31}(t) + \frac{d}{dt}\Psi_3(t) = 0
\end{gathered} \tag{21}$$

where the relationships between the line currents and the winding currents can be expressed as follows:

$$i_1 = i_{12} - i_{31}\; i_2 = i_{23} - i_{12}\; i_3 = i_{31} - i_{23} \tag{22}$$

After expressing the line currents in terms of the winding currents (for delta configuration) and rearranging, the following expression is obtained

$$\begin{gathered}
-L_{1n}\frac{d}{dt}i_{12} - L_{1s}\frac{d}{dt}i_{12}(t) - L_{2n}\frac{d}{dt}i_{12} + L_{2n}\frac{d}{dt}i_{23} + L_{1n}\frac{d}{dt}i_{31} \\
-R_{1n}i_{12} - R_{1s}i_{12}(t) - R_{2n}i_{12} + R_{2n}i_{23} + R_{1n}i_{31} \\
-\frac{d}{dt}\Psi_1(t) + u_{12}(t) = 0 \\
L_{2n}\frac{d}{dt}i_{12} - L_{2n}\frac{d}{dt}i_{23} - L_{2s}\frac{d}{dt}i_{23}(t) - L_{3n}\frac{d}{dt}i_{23} + L_{3n}\frac{d}{dt}i_{31} \\
+R_{2n}i_{12} - R_{2n}i_{23} - R_{2s}i_{23}(t) - R_{3n}i_{23} + R_{3n}i_{31} \\
-\frac{d}{dt}\Psi_2(t) + u_{23}(t) = 0 \\
L_{1s}\frac{d}{dt}i_{12}(t) + L_{2s}\frac{d}{dt}i_{23}(t) + L_{3s}\frac{d}{dt}i_{31}(t) \\
R_{1s}i_{12}(t) + R_{2s}i_{23}(t) + R_{3s}i_{31}(t) \\
+\frac{d}{dt}\Psi_1(t) + \frac{d}{dt}\Psi_2(t) + \frac{d}{dt}\Psi_3(t) = 0
\end{gathered} \tag{23}$$

Then, after isolating the designed state variables, the following set of equations is obtained

$$\begin{gathered}
-(R_{1n} + R_{1s} + R_{2n})i_{12}(t) + R_{2n}i_{23} + R_{1n}i_{31} \\
-\frac{d}{dt}\Psi_1(t) + u_{12}(t) = (L_{1n} + L_{1s} + L_{2n})\frac{d}{dt}i_{12}(t) - L_{2n}\frac{d}{dt}i_{23} - L_{1n}\frac{d}{dt}i_{31} \\
R_{2n}i_{12} - (R_{2n} + R_{2s} + R_{3n})i_{23}(t) + R_{3n}i_{31} \\
-\frac{d}{dt}\Psi_2(t) + u_{23}(t) = -L_{2n}\frac{d}{dt}i_{12} + (L_{2n} + L_{2s} + L_{3n})\frac{d}{dt}i_{23}(t) - L_{3n}\frac{d}{dt}i_{31} \\
R_{1s}i_{12}(t) + R_{2s}i_{23}(t) + R_{3s}i_{31}(t) \\
+\frac{d}{dt}\Psi_1(t) + \frac{d}{dt}\Psi_2(t) + \frac{d}{dt}\Psi_3(t) = -L_{1s}\frac{d}{dt}i_{12}(t) - L_{2s}\frac{d}{dt}i_{23}(t) - L_{3s}\frac{d}{dt}i_{31}(t)
\end{gathered} \tag{24}$$

The resulting system of equations was ordered in matrix form

$$\boldsymbol{L}\begin{bmatrix} \frac{d}{dt}i_{12} \\ \frac{d}{dt}i_{23} \\ \frac{d}{dt}i_{31} \end{bmatrix} = \boldsymbol{R}\begin{bmatrix} i_{12} \\ i_{23} \\ i_{31} \end{bmatrix} + \begin{bmatrix} -\frac{d}{dt}\Psi_1(t) \\ -\frac{d}{dt}\Psi_2(t) \\ \frac{d}{dt}\Psi_1(t) + \frac{d}{dt}\Psi_2(t) + \frac{d}{dt}\Psi_3(t) \end{bmatrix} + \begin{bmatrix} u_{12}(t) \\ u_{23}(t) \\ 0 \end{bmatrix} \tag{25}$$

where

$$\begin{aligned}
\boldsymbol{L} &= \begin{bmatrix} (L_{1n} + L_{1s} + L_{2n}) & -L_{2n} & -L_{1n} \\ -L_{2n} & (L_{2n} + L_{2s} + L_{3n}) & -L_{3n} \\ -L_{1s} & -L_{2s} & -L_{3s} \end{bmatrix} \\
\boldsymbol{R} &= \begin{bmatrix} -(R_{1n} + R_{1s} + R_{2n}) & R_{2n} & R_{1n} \\ R_{2n} & -(R_{2n} + R_{2s} + R_{3n}) & R_{3n} \\ R_{1s} & R_{2s} & R_{3s} \end{bmatrix}
\end{aligned} \tag{26}$$

In this type of modeling, the currents $i_{k,l}(t)$ of the primary windings of the transformer should be considered as additional state variables.

Finally, the state variable vector of the analyzed transformer model (see scheme in Figure 1) assumes the form:

$$\boldsymbol{X}(t) = \begin{bmatrix} x_1(t) \\ x_2(t) \\ x_3(t) \\ x_4(t) \\ x_5(t) \\ x_6(t) \end{bmatrix} = \begin{bmatrix} i_{12}(t) \\ i_{23}(t) \\ i_{31}(t) \\ \Psi_1(t) \\ \Psi_2(t) \\ \Psi_3(t) \end{bmatrix} \tag{27}$$

The system of differential equations for the state variable vector formulated in this way can be expressed as follows:

$$\frac{\mathrm{d}}{\mathrm{d}t}\boldsymbol{X}(t) = \frac{\mathrm{d}}{\mathrm{d}t}\begin{bmatrix} x_1(t) \\ x_2(t) \\ x_3(t) \\ x_4(t) \\ x_5(t) \\ x_6(t) \end{bmatrix} = \frac{\mathrm{d}}{\mathrm{d}t}\begin{bmatrix} i_{12}(t) \\ i_{23}(t) \\ i_{31}(t) \\ \Psi_1(t) \\ \Psi_2(t) \\ \Psi_3(t) \end{bmatrix} = \begin{bmatrix} f_1(\boldsymbol{X}) \\ f_2(\boldsymbol{X}) \\ f_3(\boldsymbol{X}) \\ f_4(\boldsymbol{X}) \\ f_5(\boldsymbol{X}) \\ f_6(\boldsymbol{X}) \end{bmatrix} \tag{28}$$

where

$$\begin{bmatrix} f_4(\boldsymbol{X}) \\ f_5(\boldsymbol{X}) \\ f_6(\boldsymbol{X}) \end{bmatrix} = \begin{bmatrix} R_{\mathrm{Fe},1} i_{12(p)}(t) - \frac{R_{\mathrm{Fe},1}}{N_1}\left(U_{\mathrm{m},1}(\Psi_1(t)) + R_{\mathrm{m}\delta}(\Psi_1(t) + \Psi_2(t) + \Psi_3(t))\right) \\ R_{\mathrm{Fe},2} i_{23(p)}(t) - \frac{R_{\mathrm{Fe},2}}{N_1}\left(U_{\mathrm{m},2}(\Psi_2(t)) + R_{\mathrm{m}\delta}(\Psi_1(t) + \Psi_2(t) + \Psi_3(t))\right) \\ R_{\mathrm{Fe},3} i_{31(p)}(t) - \frac{R_{\mathrm{Fe},3}}{N_1}\left(U_{\mathrm{m},3}(\Psi_3(t)) + R_{\mathrm{m}\delta}(\Psi_1(t) + \Psi_2(t) + \Psi_3(t))\right) \end{bmatrix} \tag{29}$$

and

$$\begin{bmatrix} f_1(\boldsymbol{X}) \\ f_2(\boldsymbol{X}) \\ f_3(\boldsymbol{X}) \end{bmatrix} = \boldsymbol{L}^{-1}\boldsymbol{R}\begin{bmatrix} i_{12(p)} \\ i_{23(p)} \\ i_{31(p)} \end{bmatrix} + \boldsymbol{L}^{-1}\begin{bmatrix} -f_4(\boldsymbol{X}) + u_{12}(t) \\ -f_5(\boldsymbol{X}) + u_{23}(t) \\ f_4(\boldsymbol{X}) + f_5(\boldsymbol{X}) + f_6(\boldsymbol{X}) \end{bmatrix} \tag{30}$$

In this way, a general state system was obtained in the form of nonlinear differential Equations (29) and (30), describing the updated transformer model.

8. Measurements and Simulations of Transformer Inrush Dynamics

8.1. Positive Pre-Magnetization

As demonstrated in studies [3,24], when a transformer is connected to the grid, current pulses appear during the first cycle of the voltage waveform. Their maximum values significantly exceed the nominal values. Therefore, if the analysis of the transformer's transient state is limited to the first voltage cycle, using the proposed model with the specified initial conditions enables a detailed investigation of the impact of these current pulses, particularly in relation to residual magnetism [39].

Subsequently, a comparative analysis was conducted between the waveforms of the current pulses $i_{k,l(\mathrm{sim})}(t)$ (determined numerically) and the discrete (recorded) measurement currents $i_{k,l(\mathrm{meas})}(t)$. These were analyzed for different time instances Δt, measured from the time instant when the voltage $u_{23}(t)$ crosses zero, and for specific pre-magnetization of the transformer columns in the proportion $B_1 = -\frac{1}{2}B_0$, $B_2 = B_0$, $B_3 = -\frac{1}{2}B_0$ (see (3)).

The measurements were performed using the proprietary systems shown in Figures 2 and 6, which incorporated the capability to control the timing of the voltage application to the transformer. In the experiment, 36 transformer switch-ons were carried out at intervals of $\frac{\mathrm{T}}{36}$ s, where T is the period of the supply voltage. In each computational cycle, the core is magnetized by a set magnetized current (see Figure 2 and Equation (2)); then, this current is switched off and the thyristor switch is activated.

The graphs of the instantaneous values of the inrush currents with positive magnetization are shown in Figures 12–14.

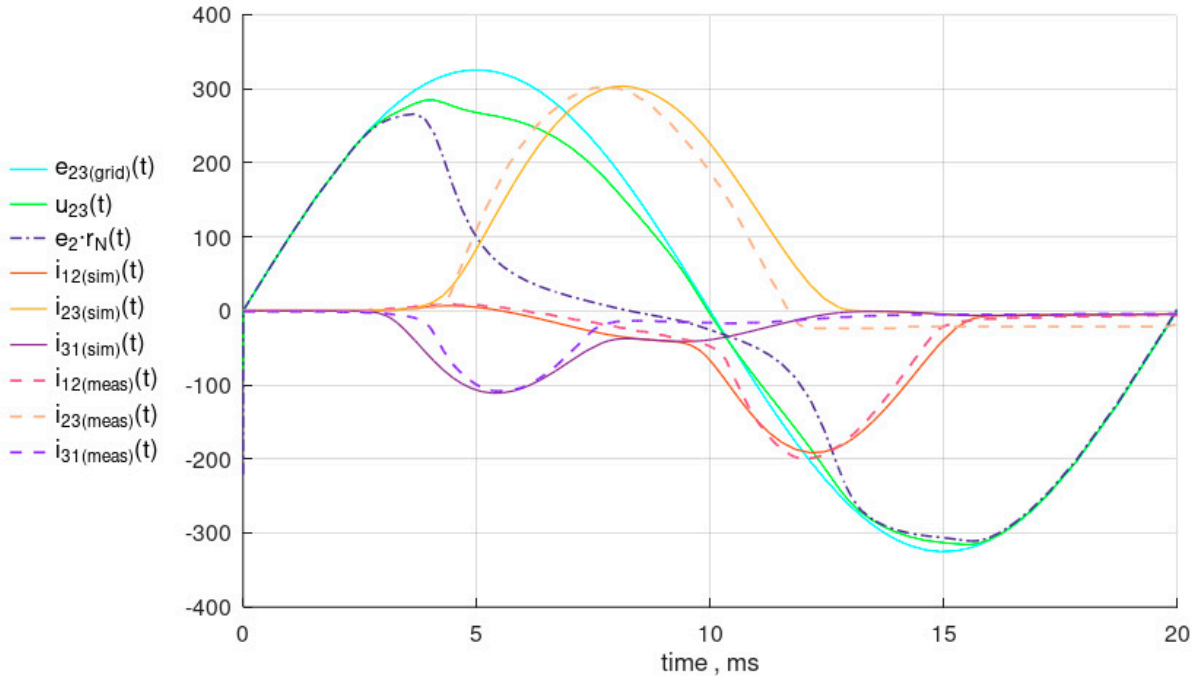


Figure 12. Comparison of instantaneous values of currents $i_{k,l(\mathrm{sim})}(t)$ (numerically determined) with the discrete values of measured currents $i_{k,l(\mathrm{meas})}(t)$; transformer is energized immediately after voltage $u_{23}(t)$ crosses zero; initial magnetization values set at the proportion $B_1 = -0.5\,\mathrm{T}$, $B_2 = 1.0\,\mathrm{T}$, $B_3 = -0.5\,\mathrm{T}$; the current waveforms are magnified 10 times for readability's sake.

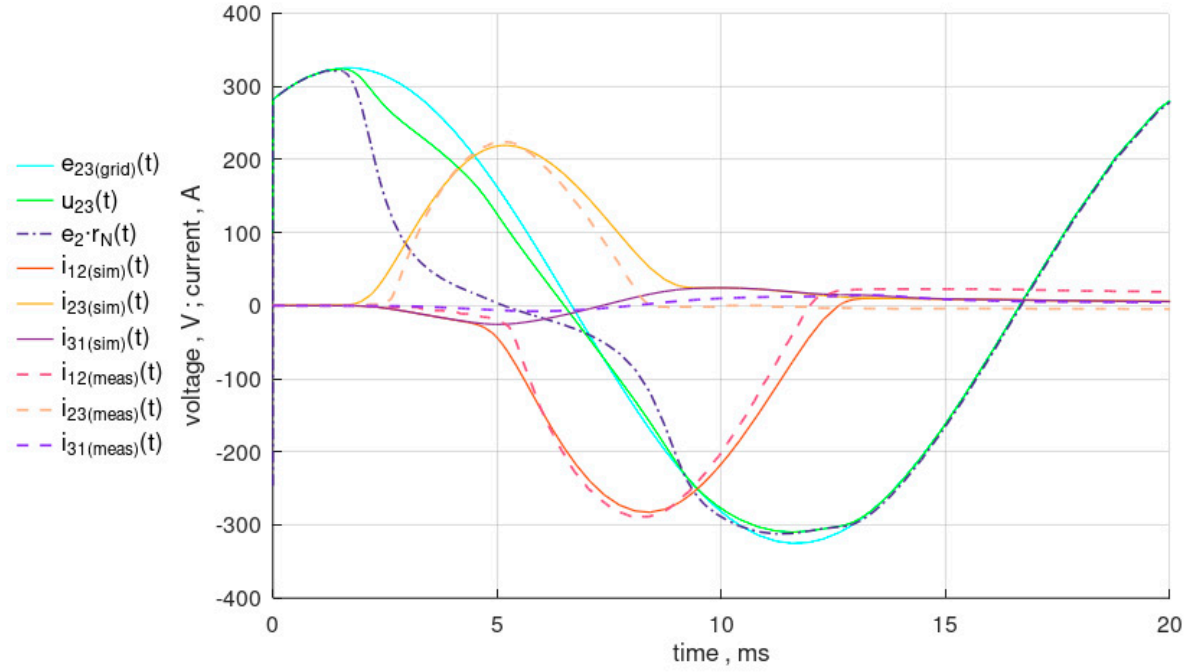


Figure 13. Comparison of the instantaneous values of currents $i_{k,l(\mathrm{sim})}(t)$ (numerically determined) with the discrete values of measured currents $i_{k,l(\mathrm{meas})}(t)$; transformer is energized after one-sixth ($\frac{\mathrm{T}_0}{6}$) of the supply voltage period T_0, counting from the time instant when voltage $u_{23}(t)$ crosses zero; initial magnetization values set at $B_1 = -0.5\,\mathrm{T}$, $B_2 = 1.0\,\mathrm{T}$, $B_3 = -0.5\,\mathrm{T}$; the current waveforms are magnified 10 times for readability's sake.

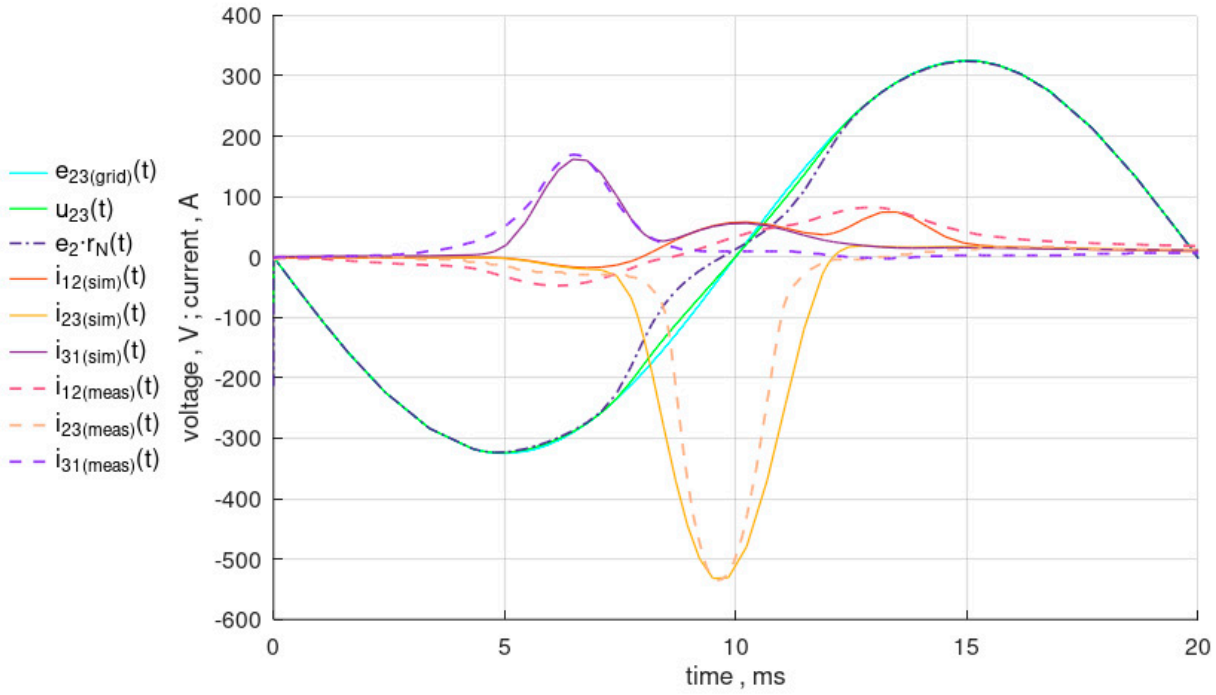


Figure 14. Comparison of instantaneous values of currents $i_{k,l(\mathrm{sim})}(t)$ (numerically determined) with the discrete values of measured currents $i_{k,l(\mathrm{meas})}(t)$; transformer is energized after half ($\frac{\mathrm{T}_0}{2}$) of the supply voltage period T_0, counting from the time instant when voltage $u_{23}(t)$ crosses zero; initial magnetization set at $B_1 = -0.5\,\mathrm{T}, B_2 = 1\,\mathrm{T}, B_3 = -0.5\,\mathrm{T}$; the current waveforms are magnified 100 times for readability's sake.

Analyzing the obtained results, it can be observed that current pulses (Figure 14) of small magnitude occur when the transformer is energized at the time instant $\frac{\mathrm{T}_0}{2}$; this is set in relation to reference voltage $u_{23}(t)$, when the voltage passes from negative to positive values. This takes place with the magnetization of core columns set as follows (positive magnetization) $B_1 = -0.5\,\mathrm{T}, B_2 = 1\,\mathrm{T}, B_3 = -0.5\,\mathrm{T}$.

To illustrate the full spectrum of emerging patterns, a set of characteristics of the maximum current values in the first period of the transient state as a function dependent on the time instant when the voltage $u_{23}(t)$ crosses zero from negative to positive values was compiled; initial magnetization B_0 (Figure 15) was set at different values.

In the analysis, a norm was adopted for determining the maximum current value in a three-phase system in the form of the relationship

$$I_{\max}(B_0) = \max_{t\in[0,\mathrm{T}]}\{|i_{12}(t)|, |i_{23}(t)|, |i_{31}(t)|\} \tag{31}$$

The calculations and measurements shown in Figure 15 show that the minimum values of $I_{\max}(B_0)$ occur at a time $\Delta t = 10\,\mathrm{ms}$ after the reference sine voltage $u_{23}(t)$ crosses zero, passing from negative to positive values. However, this minimum depends on the magnitude of the initial magnetization B_0. For $B_0 = 0$, the maximum current $I_{\max}(B_0)$ reaches its highest value, whereas for $B_0 = 1.0\,\mathrm{T}$, the inrush current of the transformer under no-load conditions is practically reduced to the rated current of the transformer. This general trend is confirmed by the measurement curve of the recorded maximum values superimposed over the family of calculated characteristics (Figure 15).

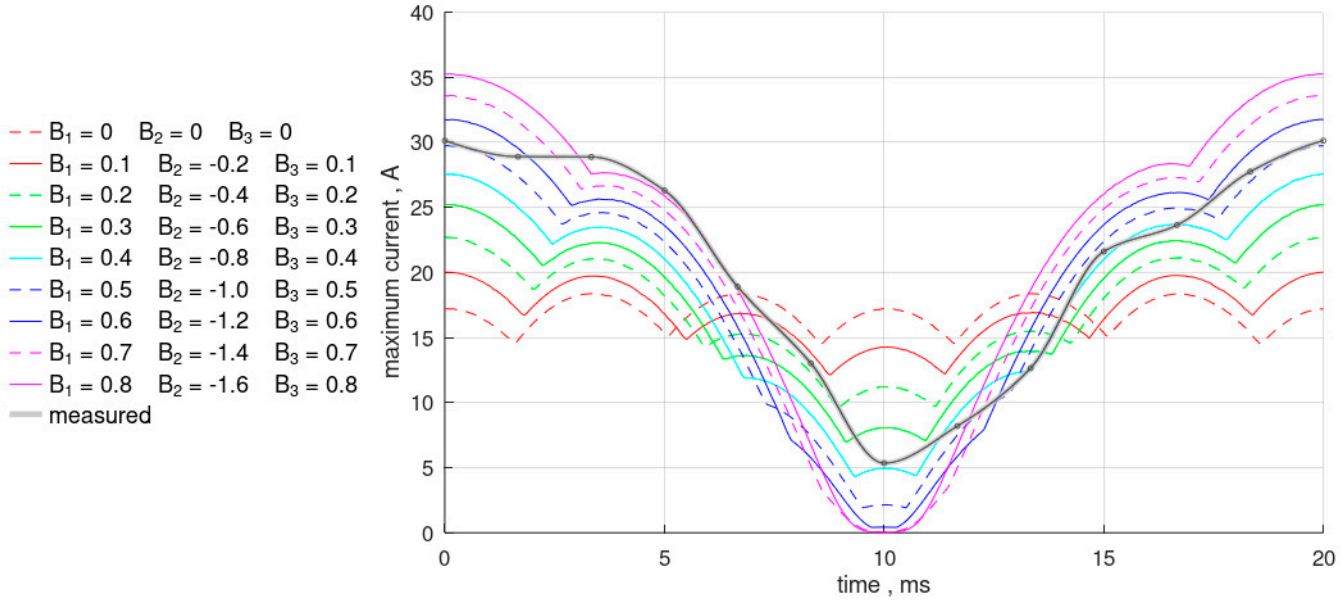


Figure 15. Comparison of the maximum current pulse values for different energizing times Δt of the voltage applied to the transformer, measured relative to the time instant when the voltage $u_{23}(t)$ crosses zero, for various magnetization values $B_0 = \text{var}$ with the proportions $B_1 = -0.5\,B_0, B_2 = B_0$, $B_3 = -0.5\,B_0$ in relation to the measurement data.

8.2. Negative Pre-Magnetization

To demonstrate and verify the impact of reverse initial magnetization of the transformer's core columns with proportions (10), a similar experiment was conducted. Once again, 36 transformer energizations were carried out at intervals of $\frac{\mathrm{T}}{36}$ seconds to perform a comparative analysis of the current pulse waveforms $i_{k,l(\mathrm{sim})}(t)$ (numerically determined) with the discrete values of measured currents $i_{k,l(\mathrm{meas})}(t)$ during the energizing of the transformer at different time instants Δt measured from the time instant when the voltage $u_{23}(t)$ crosses zero, as well as for the given magnetization levels of the transformer columns. This time, in each calculation cycle, the system undergoes magnetization by setting the magnetizing current in such a way that its sudden disconnection establishes the magnetization level within the limits with thr proportions $B_1 = 0.5\,B_0, B_2 = -B_0\,, B_3 = 0.5\,B_0$.

The graphs of selected instantaneous inrush current values at negative initial magnetization are shown in Figures 16 and 17.

Using the previously validated norm $I_{\max}(B_0) = \max\limits_{t\in[0,\mathrm{T}]}\{|i_{12}(t)|, |i_{23}(t)|, |i_{31}(t)|\}$, calculations were carried out to analyze the entire spectrum of the maximum inrush current values during the first period of the transient state. This function consistently depended on the time instant when the voltage $u_{23}(t)$ crossed zero from negative to positive values for different levels of initial magnetization B_0 (Figure 18).

As indicated by the collected simulation results compared with the measurement data (Figure 18), the minimum values of $I_{\max}(B_0)$ occur at the time instant Δt when the voltage $u_{23}(t)$ crosses zero. This minimum, however, depends on the level of initial magnetization B_0. For $B_0 = 0$, the maximum current $I_{\max}(B_0)$ reaches its highest value, whereas for $B_0 = 1.0\,\mathrm{T}$, the inrush current of the transformer under no-load conditions is practically reduced to the rated current. This trend is once again confirmed by the curve representing the measurements of maximum current values superimposed over the family of calculated characteristics (Figure 18).

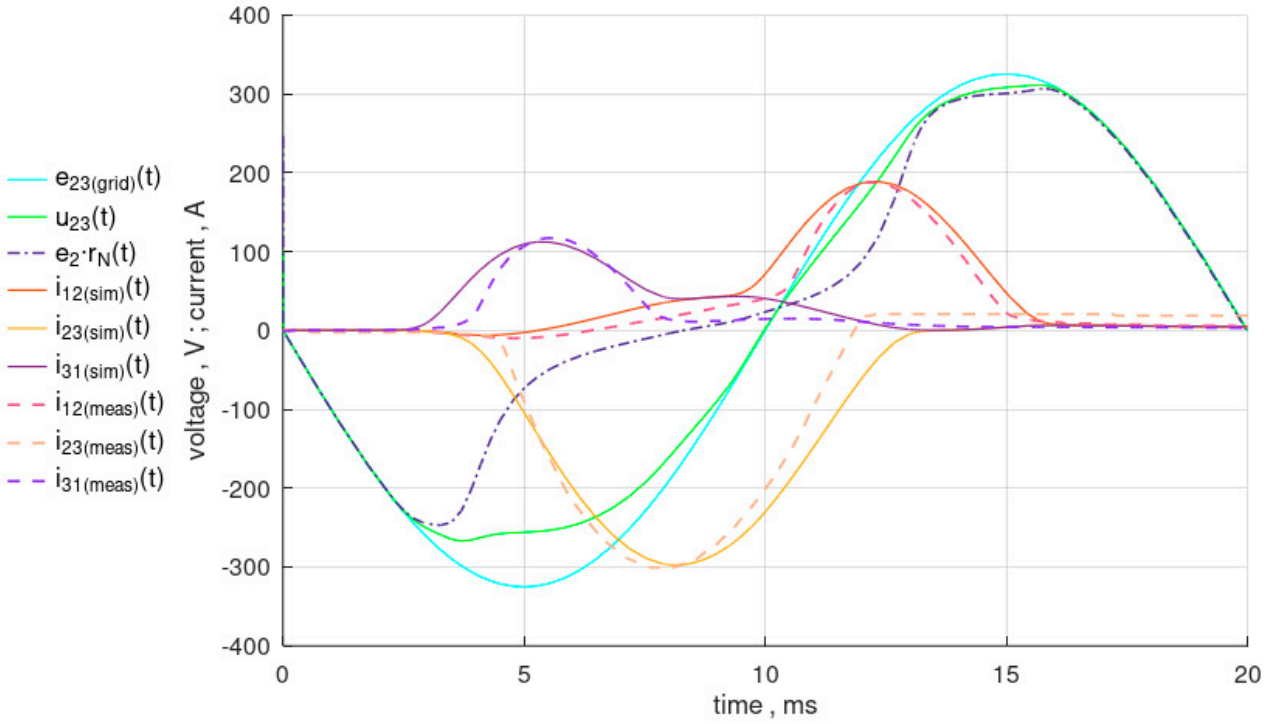


Figure 16. Comparison of instantaneous values of currents $i_{k,l(\mathrm{sim})}(t)$ (numerically determined) with the discrete values of measured currents $i_{k,l(\mathrm{meas})}(t)$ during the energizing of the transformer and after half of the supply voltage period $\Delta t = \frac{T_0}{2}$ counted from the time instant when the voltage $u_{23}(t)$ crosses zero; initial magnetization values set in proportions $B_1 = 0.5\,\mathrm{T}, B_2 = -1\,\mathrm{T}, B_3 = 0.5\,\mathrm{T}$; the current waveforms are magnified 10 times for readability's sake.

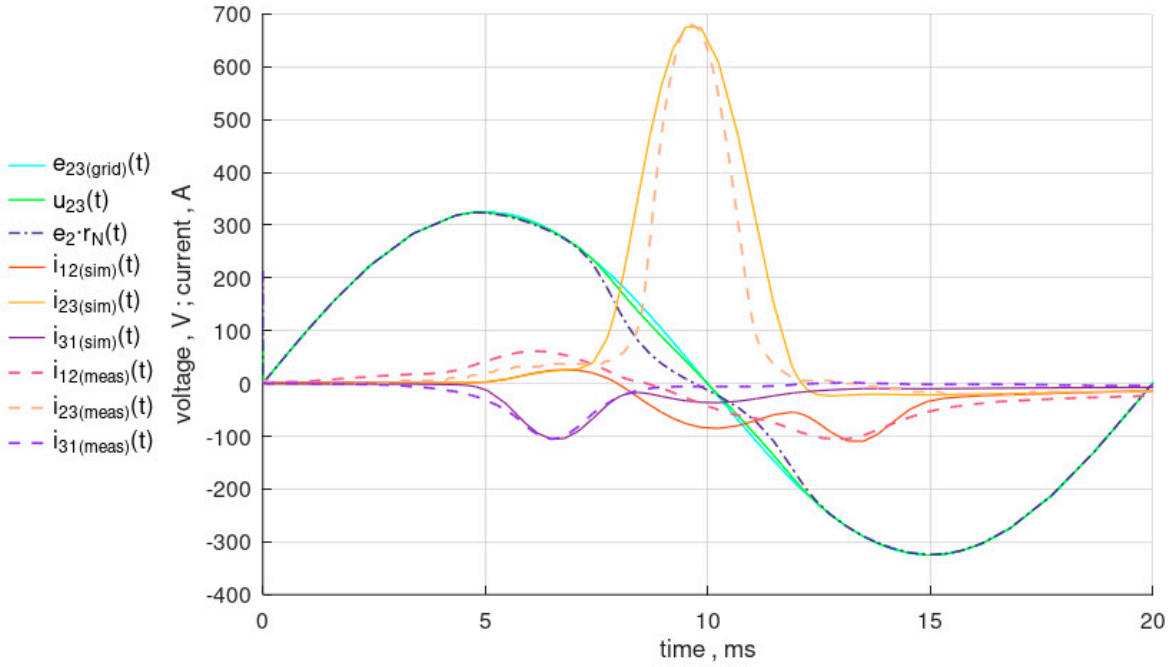


Figure 17. Comparison of the instantaneous values of currents $i_{k,l(\mathrm{sim})}(t)$ (numerically determined) with the discrete values of measured currents $i_{k,l(\mathrm{meas})}(t)$; transformer is energized immediately after voltage $u_{23}(t)$ crosses zero; initial magnetization values set in proportion $B_1 = 0.4\,\mathrm{T}, B_2 = -0.8\,\mathrm{T}$, $B_3 = 0.4\,\mathrm{T}$; the current waveforms are magnified 100 times for readability's sake.

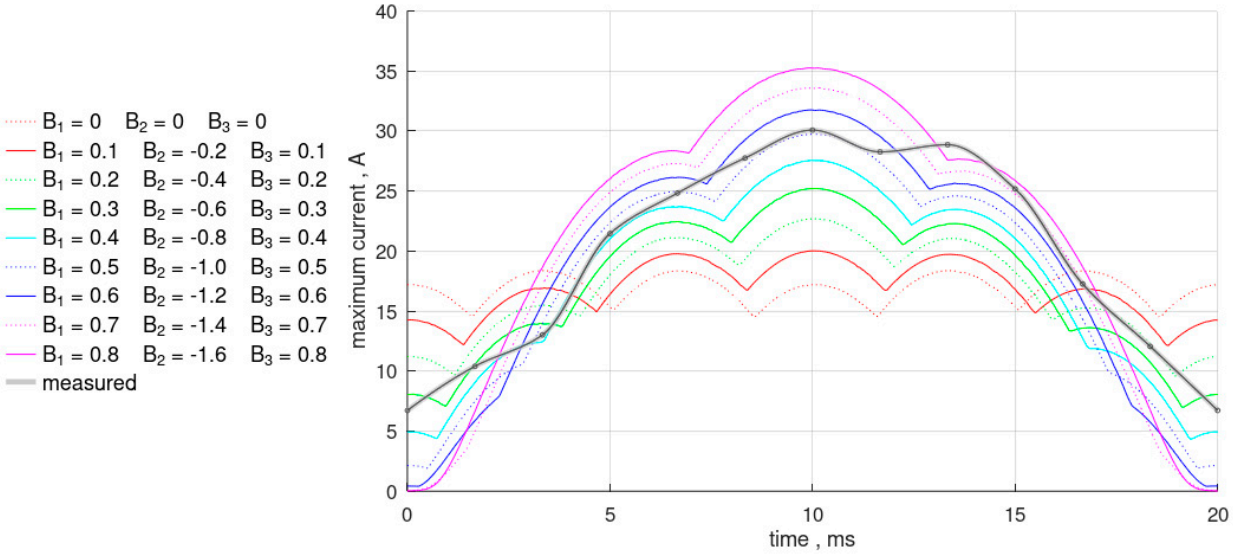


Figure 18. Comparison of the maximum current pulse values for different energizing times Δt of the voltage applied to the transformer, measured relative to the time instant when the voltage $u_{23}(t)$ crosses zero, for various magnetization values $B_0 = \text{var}$ with the proportions $B_1 = 0.5\,B_0$, $B_2 = -B_0$, $B_3 = 0.5B_0$ in relation to the measurement data.

The comparison between measurements and calculations (Figures 15 and 18) shows that such a sudden disconnection of the magnetizing current stabilizes the magnetization level within the range of 0.8 T to 1.0 T.

9. Systematization of the Obtained Results

Comparing the families of instantaneous values of winding currents shown in Figures 12–17, it can be observed that the current pulses are almost identical as to the absolute value (in pairs), but their polarity is opposite (the entire group)—Figure 19.

When Figures 12 and 16 and Figures 14 and 17 are compared, interesting patterns can be observed. The figures, when arranged in these combinations, exhibit very clear similarities. They are mirror images with respect to the time axis. The amplitudes of the current pulses, their phase sequence, and even the distortions visible in the waveforms of the induced voltages on the secondary side of the transformer remain nearly identical.

Figure 12 presents the transformer's energization with a zero-phase reference voltage and positive magnetization in the central core. Figure 16 illustrates the change induced by reversing the polarity of the magnetization in the central core and introducing a phase shift in the reference voltage by $\frac{T_0}{2}$, resulting in a mirror image with respect to the time axis when compared to Figure 12.

The same regularity is demonstrated by the comparison of Figures 14 and 17; this takes into account a similar simultaneous change in both factors. Figure 14 illustrates the energization at a reference voltage, an initial phase of 180 degrees, and through positive magnetization. The mirror effect (Figure 17) is achieved by reversing the polarity of the magnetization $B_2 = -B_0$ and energizing the transformer at the instant the reference voltage crosses zero.

It is crucial to emphasize that, in both of these combinations, a constant reference system is assumed for calculating the energization moment (initial phase, the time instant at which the switch-on takes place) of the reference voltage, represented by its transition from negative to positive values ($-/+$). Disrupting this reference system immediately introduces chaos. Referring again to Figure 12 (positive magnetization and energization with zero-phase at the reference voltage's $-/+$ transition), the result in Figure 16 can be achieved merely by reversing the magnetization polarity (negative) without the need for a

$\frac{T_0}{2}$ phase shift. This effect will naturally occur due to the change in the reference system, where the voltage transitions from +/−.

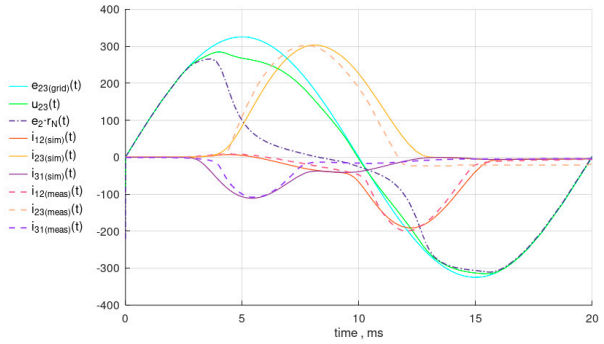


Figure 12 $i(t)\cdot 10$ $B_2 = B_0$ $\Delta t = 0$

$u_{23}(t)$ {−/+} ; $(\frac{d}{dt}u_{23}(t) > 0)$

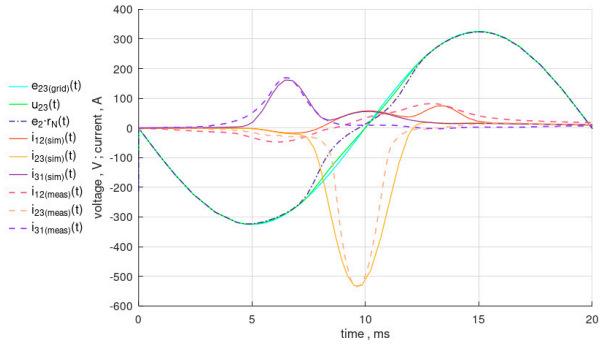


Figure 14 $i(t)\cdot 100$ $B_2 = B_0$ $\Delta t = \frac{T_0}{2}$

$u_{23}(t)$ {−/+} ; $(\frac{d}{dt}u_{23}(t) > 0)$

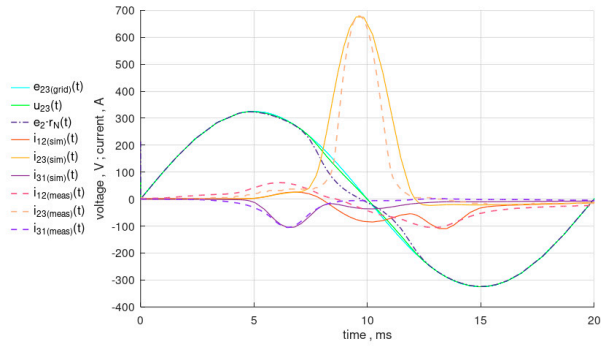


Figure 17 $i(t)\cdot 100$ $B_2 = -B_0$ $\Delta t = 0$

$u_{23}(t)$ {−/+} ; $(\frac{d}{dt}u_{23}(t) > 0)$

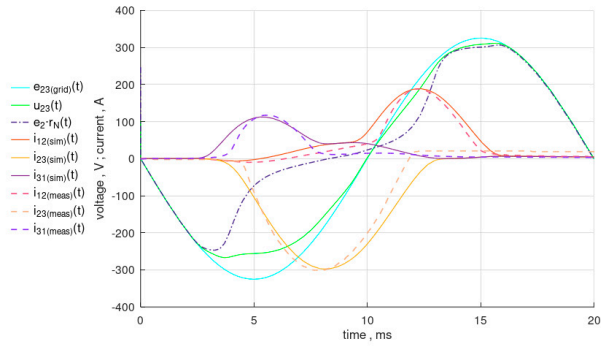


Figure 16 $i(t)\cdot 10$ $B_2 = -B_0$ $\Delta t = \frac{T_0}{2}$

$u_{23}(t)$ {−/+} ; $(\frac{d}{dt}u_{23}(t) > 0)$

Figure 19. Comparison of the transformer's selected inrush scenarios (both measured and simulated); the characteristic values corresponding to the parameters defining each scenario are summarized in the table below each waveform.

The above findings finally allow us to address the most crucial aspect—the minimization of inrush current during the energization of an unloaded three-phase Dy transformer.

Taking into account Figures 12 and 14 and Figures 16 and 17, and keeping in mind that a constant reference system is applied (the transition of the reference voltage from −/+) and that magnetization polarity does not change, it may be observed that the time difference between the maximum and minimum inrush current values is always $\frac{T_0}{2}$.

Energizing with a zero-phase reference voltage (Figure 12) and positive magnetization results in the highest maximum inrush current values. Shifting the energization moment by $\frac{T_0}{2}$ in the reference voltage reduces this value to the minimum (Figure 14). The same effect can be achieved merely by changing the magnetization polarity without altering the energization time instant (still at zero-phase)—(Figure 17).

For energization with an initial phase of $\frac{T_0}{2}$, this pattern differs only in the polarity of the resulting waveform (a mirror image with respect to the time axis).

Naturally, in all the aforementioned patterns, one cannot overlook the documented symmetry, namely $B_2 = B_0$ and $B_1 = B_3 = \frac{B_0}{2}$, as well as the value of B_0 (assumed to be approx. 1 T)—Figures 15 and 18.

10. Final Conclusions

The article presents an original (authorial) strategy for reducing the inrush current of a three-phase Dy transformer. The concept of the strategy is based on the successful combination of two tightly controlled procedures: −1—preliminary magnetization of the transformer's columns in specific proportions and with a defined polarity; −2—controlled switching at a precisely determined time instant. The methodology, measurement and research (simulation) procedures, as well as the detailed structure of the developed control systems presented in the article, are the culmination of successful mathematical modeling studies (described in series of publications [23–25]) and offer a ready-to-implement solution.

Moreover, the article presents the results of experimental verification of the developed strategy. The research was conducted on a real object, and the results were intentionally compared with those obtained from mathematical modeling. The high consistency between the waveforms obtained through calculations and those recorded on the tested transformer confirms the effectiveness of the developed strategy in reducing the inrush current pulses generated when an unloaded three-phase Dy transformer is switched on. It is worth emphasizing that this particular connection group (Dy) of three-phase transformers is widely applied in power engineering, especially in transmission and distribution networks.

The model of the transformer proposed by the authors allows for a wide range of simulation possibilities, enabling the analysis of the impact of almost any variable among those describing the transformer on the value of the inrush current generated during the first cycle of the supply voltage. The possibilities range from physical parameters, such as the ferromagnetic core properties and the number of turns, to the simulation-based control of the pre-magnetization of individual columns in arbitrary proportions and polarities, as well as the manipulation of the time instants at which the voltage is applied.

In the model, a single equivalent element was adopted to represent the influence of all three columns during the transient state that occurs when the unloaded transformer is energized. The shunt is considered common to all three phases, which exhibit significant asymmetry at this particular moment. The value of the reluctance $R_{m\delta}$ obtained through estimation is therefore an average for all three phases (see Figure 11 and observe the lack of complete conformity between the waveforms used to estimate the value of the reluctance $R_{m\delta}$ adopted in the mathematical model). While this could seemingly be perceived as a weakness of the circuit model (compared to, for example, a field model), it is worth noting how excellently the considered model managed to replicate the current pulse maxima in all scenarios and phases (at a significantly lower computational cost compared to a potential field model).

Furthermore, the mathematical apparatus employed, specifically dedicated to solving stiff equations, allows for rapid calculations of the steady state (using an approximate solution of nonlinear differential equations).

The scope of the study is complete, experimentally verified, and ready for further exploratory work. Moreover, the solution is complete and verified on a real object. In the authors' opinion, this constitutes a novelty of this study compared to previous works. The proposed solution is primarily addressed to professional engineers.

In conclusion, with regard to the most important substantive aspect of the research—the reduction in inrush currents in the Dy transformer switch-on without load—it should be noted that, from the obtained pairs of recurring distributions of maximum current pulse values for different voltage switching times Δt on the transformer, two clearly yield minimal values:

1. With preliminary magnetization, as shown in Figure 2, where the proportions are $B_1 = 0.5\,B_0, B_2 = -B_0, B_3 = 0.5\,B_0$, the transformer should be energized when the voltage $u_{23}(t)$ crosses zero from negative to positive values, i.e., when $\frac{\mathrm{d}}{\mathrm{d}t}u_{23}(t) > 0$.
2. With preliminary magnetization, as shown in Figure 2, where the proportions are $B_1 = -0.5\,B_0, B_2 = B_0, B_3 = -0.5\,B_0$, the transformer should be energized at the moment when the voltage $u_{23}(t)$ crosses zero from positive to negative values, i.e., when $\frac{\mathrm{d}}{\mathrm{d}t}u_{23}(t) < 0$.

This means that there are two practical methods for connecting the transformer to the grid where the preliminary magnetization results in minimal inrush current pulses. Considering the practical applications of the obtained results, it is crucial to take into account the aforementioned pairs of distributions (solutions).

The value of the initial magnetization B_0 can be set using the system shown in Figure 2. In this system, the magnetization maintains a symmetry characterized by maximum magnetization in the central column of the transformer, while, in the outer columns, it is half as strong and of an opposite polarity. Maintaining this specific symmetry during preliminary magnetization is crucial as it ensures minimal (reduced) inrush current values for the transformer regardless of the phase sequence of the power supply system.

The implementation of the developed strategy can significantly reduce the inrush currents of a three-phase Dy power transformer, which should be considered a step to improvement in the efficiency and stability of the power system.

Author Contributions: Conceptualization, M.Ł., Ł.M. and B.B.; methodology, Ł.M., B.B., K.T. and K.W.; software, B.B. and K.W.; validation, M.Ł., K.T. and K.W.; formal analysis, Ł.M., B.B. and B.K.; investigation, Ł.M., B.B. and K.W.; resources, Ł.M. and K.T.; data curation, B.K. and K.W.; writing—original draft preparation, Ł.M., B.B. and K.W.; writing—review and editing, M.Ł., Ł.M., B.K. and K.T.; visualization, Ł.M., B.B. and K.W.; supervision, M.Ł., B.K. and K.T.; project administration, M.Ł., B.K. and K.T.; funding acquisition, M.Ł. All authors have read and agreed to the published version of the manuscript.

Funding: This research received no external funding.

Data Availability Statement: Available on demand.

Acknowledgments: This paper is a result of the scientific internship accomplished by Łukasz Majka at the Opole University of Technology.

Conflicts of Interest: The authors declare no conflicts of interest.

Abbreviations

The list of symbols and notations used in this paper:

r_{N}	turns ratio of transformer
N_1	number of turns of primary winding
N_2	number of turns of secondary winding
$i_{k,l(\mathrm{p})}(t)$	no-load current in the primary winding of the transformer
$u_{k,l(\mathrm{p})}(t)$	sinusoidal waveform of supplied voltage
φ_0	initial phase of the supplied voltage
$e_{k(\mathrm{s})}(t)$	the electromotive force (emf) induced in the secondary winding
$R_{\mathrm{Fe},k}$	iron core resistance
R_{sk}	primary winding resistance
L_{sk}	primary leakage inductance
$\Psi_k(t)$	flux leakage
B	magnetic flux density
H	magnetic field strength
$U_{\mathrm{m},k}$	magnetic voltage drop
$\Theta_1(t)$	magnetomotive force (mmf) of individuals transformers coils
$R_{\mathrm{m}\delta}$	air shunt magnetic resistance
s_{Fe}	cross-sectional area of the core of the transformer

References

1. Sung, B.C.; Kim, S. Accurate transformer inrush current analysis by controlling closing instant and residual flux. *Electr. Power Syst. Res.* **2023**, *223*, 109638. [CrossRef]
2. Sanati, S.; Ahmadi, S.-A.; Sanaye-Pasand, M. An innovative harmonic-based approach for inrush current detection in low-loss transformers. *IET Gener. Transm. Distrib.* **2024**, *18*, 1303–1316. [CrossRef]
3. Aghazadeh, A.; Hajipour, E.; Li, K.; Azizi, S. Mitigating the Inrush Current of V/V Transformers Using Railway Conditioners. *IEEE Access* **2024**, *12*, 50885–50897. [CrossRef]
4. Steurer, M.; Fröhlich, K.J. The impact of inrush currents on the mechanical stress of high voltage power transformer coils. *IEEE Trans. Power Del.* **2002**, *17*, 155–160. [CrossRef]
5. Zhang, C.; Ge, W.; Xie, Y.; Li, Y. Comprehensive analysis of winding electromagnetic force and deformation during no-load closing and short-circuiting of power transformers. *IEEE Access* **2021**, *9*, 73335–73345. [CrossRef]
6. Dashti, H.; Davarpanah, M.; Sanaye-Pasand, M.; Lesani, H. Discriminating transformer large inrush currents from fault currents. *Int. J. Electr. Power Energy Syst.* **2017**, *75*, 74–82. [CrossRef]
7. Mishra, A.; Swain, A.; Pradhan, K.; Bajpai, P. Sequence currentbased inrush detection in high-permeability core transformers. *IEEE Trans. Instrum. Meas.* **2023**, *72*, 3534509. [CrossRef]
8. Liu, P.; Jiao, B.; Zhang, P.; Du, S.; Zhu, J.; Song, Y. Countermeasure to prevent transformer differential protection from false operations. *IEEE Access* **2023**, *11*, 45950–45960. [CrossRef]
9. Sahebi, A.; Samet, H.; Ghanbari, T. Evaluation of power transformer inrush currents and internal faults discrimination methods in presence of fault current limiter. *Renew. Sustain. Energy Rev.* **2017**, *68*, 102–112. [CrossRef]
10. Fang, S.; Ni, H.; Lin, H.; Ho, S.L. A novel strategy for reducing inrush current of three-phase transformer considering residual flux. *IEEE Trans. Ind. Electr.* **2016**, *63*, 4442–4451. [CrossRef]
11. Hagh, T.; Valizadeh, M. Analysis and comparative study of transient inrush current reduction methods. In Proceedings of the 2007 International Power Engineering Conference (IPEC 2007), Singapore, 3–6 December 2007; pp. 287–291.
12. Tseng, H.-T.; Chen, J.-F. Voltage compensation-type inrush current limiter for reducing power transformer inrush current. *IET Electr. Power Appl.* **2012**, *6*, 101–110. [CrossRef]
13. Ketabi, A.; Zavareh, A.R.H. New method for inrush current mitigation using series voltage-source PWM converter for three phase transformer. In Proceedings of the 2011 2nd Power Electronics, Drive Systems and Technologies Conference, Tehran, Iran, 16–17 February 2011; pp. 501–506.
14. Alassi, A.; Ahmed, K.H.; Egea-Alvarez, A.; Foote, C. Transformer Inrush Current Mitigation Techniques for Grid-Forming Inverters Dominated Grids. *IEEE Trans. Power Deliv.* **2023**, *38*, 1610–1620. [CrossRef]
15. Pan, Y.; Yin, X.; Zhang, Z.; Liu, B.; Wang, M.; Yin, X. Three-phase transformer inrush current reduction strategy based on prefluxing and controlled switching. *IEEE Access* **2021**, *9*, 38961–38978. [CrossRef]
16. Cui, Y.; Abdulsalam, S.G.; Chen, S.; Xu, W. A sequential phase energization technique for transformer inrush current reduction—Part I: Simulation and experimental results. *IEEE Trans. Power Del.* **2005**, *20*, 943–949. [CrossRef]
17. Xu, W.; Abdulsalam, S.G.; Cui, Y.; Liu, X. A sequential phase energization technique for transformer inrush current reduction—Part II: Theoretical analysis and design guide. *IEEE Trans. Power Del.* **2005**, *20*, 950–957. [CrossRef]
18. Parikh, U.; Bhavesh, R.B. Mitigation of magnetic inrush current during controlled energization of coupled un-loaded power transformers in presence of residual flux without load side voltage measurements. *Int. J. Electr. Power Energy Syst.* **2016**, *76*, 156–164. [CrossRef]
19. Cano-González, R.; Bachiller-Soler, A.; Rosendo-Macías, J.A.; Álvarez-Cordero, G. Controlled switching strategies for transformer inrush current reduction: A comparative study. *Electr. Power Syst. Res.* **2017**, *145*, 12–18. [CrossRef]
20. Sahoo, S.K.; Modi, A.; Balamurugan, M.; Sultana, R.; Chhawchharia, S. Reduction of inrush current using point on wave switching in power transformers. In Proceedings of the Innovations in Power and Advanced Computing Technologies, Vellore, India, 21–22 April 2017.
21. Li, Y.; Zhao, C.; Jiang, H.; Zhang, Y.; Muljadi, E. *New Technologies for Power System Operation and Analysis*; Jiang, H., Zhang, Y., Muljadi, E., Eds.; Academic Press: Cambridge, MA, USA, 2021.
22. Sodhi, R. *Simulation and Analysis of Modern Power Systems*; McGraw Hill Education: New York, NY, USA, 2021.
23. Łukaniszyn, M.; Majka, Ł.; Baron, B.; Sowa, M.; Tomczewski, K.; Wróbel, K. Practical Experiments with a Ready-Made Strategy for Energizing a Suitable Pre-Magnetized Three-Column Three-Phase Dy Transformer in Unloaded State for Inrush Current Computations. *Energies* **2024**, *17*, 2298. [CrossRef]
24. Łukaniszyn, M.; Baron, B.; Kolańska-Płuska, J.; Majka, Ł. Inrush Current Reduction Strategy for a Three-Phase Dy Transformer Based on Pre-Magnetization of the Columns and Controlled Switching. *Energies* **2023**, *16*, 5238. [CrossRef]
25. Majka, Ł.; Baron, B.; Zydroń, P. Measurement-based stiff equation methodology for single phase transformer inrush current computations. *Energies* **2022**, *15*, 7651. [CrossRef]
26. Baron, B.; Kolańska-Płuska, J.; Łukaniszyn, M.; Spałek, D.; Kraszewski, T. Solution of nonlinear stiff differential equations for a three-phase no-load transformer using a Runge-Kutta implicit method. *Arch. Electr. Eng.* **2022**, *71*, 1081–1106.
27. Ren, Y.; Liu, C.; Wang, Y. Residual flux density estimation of the three-phase transformer using BP neural network. *AIP Adv.* **2024**, *14*, 015036. [CrossRef]

28. Peng, T.; Wan, D.; Zhao, M.; Zhou, H.; Mao, L.; Duan, X. An Indirect Method for Measuring Transformer Residual Magnetism. In Proceedings of the IEEE 3rd Conference on Energy Internet and Energy System Integration (EI2), Changsha, China, 8–10 November 2019; pp. 1084–1087.
29. Huo, C.; Wu, S.; Yang, Y.; Liu, C.; Wang, Y. Residual flux density measurement method of single-phase transformer core based on time constant. *IEEE Access* **2020**, *8*, 171479–171488. [CrossRef]
30. Zhang, H.; Long, J.; Li, X.; Xu, Y.; Shi, J.; Ren, L.; Yang, W.; Wang, Z.; Chen, M. A new method to measure the residual flux by magnetic sensors and a finite-element model. *IEEE Trans. Instrum. Meas.* **2023**, *72*, 6006010. [CrossRef]
31. Majka, Ł.; Szuster, D. Application of the stationary DC decay test to industrial turbogenerator model parameter estimation. *Przegl. Elektrotechniczny* **2014**, *90*, 242–245.
32. Chwastek, K.; Najgebauer, M.; Jabłoński, P.; Szczegielniak, T.; Kusiak, D.; Koprivica, B.; Rosić, M.; Divac, S. Modeling Dynamic Hysteresis Curves in Amorphous Magnetic Ribbons. *Appl. Sci.* **2023**, *13*, 9134. [CrossRef]
33. Ge, W.; Wang, Y.; Zhao, Z.; Yang, X.; Li, Y. Residual Flux in the Closed Magnetic Core of a Power Transformer. *IEEE Trans. Appl. Supercond.* **2014**, *24*, 0502404.
34. Lewandowski, M.; Majka, Ł. Combining optimal SASS (Sparsity Assisted Signal Smoothing) and notch filters for transient measurement signals denoising of large power generating unit. *Measurement* **2024**, *237*, 270749124. [CrossRef]
35. Zheng, Y.-P.; Zhang, Z.-Y.; Wang, C.-H.; Pan, S.-Y. Leakage Flux-Based Method to Identify the Inrush Current in Transformers. In Proceedings of the 12th International Conference on Measuring Technology and Mechatronics Automation (ICMTMA), Phuket, Thailand, 28–29 February 2020; pp. 1083–1088.
36. Sowa, M.; Majka, Ł.; Wajda, K. Excitation system voltage regulator modeling with the use of fractional calculus. *AEU Int. J.Electron. Commun.* **2023**, *159*, 154471. [CrossRef]
37. Sowa, M. Ferromagnetic coil frequency response and dynamics modeling with fractional elements. *Electr. Eng.* **2021**, *103*, 1737–1752. [CrossRef]
38. Hairer, E.; Wanner, G. *Solving Ordinary Differential Equations II: Stiff and Differential-Algebraic Problems*, 2nd ed.; Springer: Berlin/Heidelberg, Germany, 2010.
39. Ge, W.; Zhao, J.; Wang, Y. Analysis of the residual flux influence on inrush current and electromagnetic force in large power transformer. *J. Eng.* **2019**, *11*, 2426–2429. [CrossRef]

Disclaimer/Publisher's Note: The statements, opinions and data contained in all publications are solely those of the individual author(s) and contributor(s) and not of MDPI and/or the editor(s). MDPI and/or the editor(s) disclaim responsibility for any injury to people or property resulting from any ideas, methods, instructions or products referred to in the content.